Marine and Petroleum Geology 171 (2025) 107158

Contents lists available at ScienceDirect

Marine and Petroleum Geology

journal homepage: www.elsevier.com/locate/marpetgeo

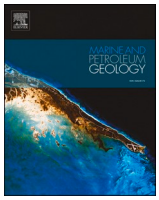

Late Triassic to present-day tectono-thermal history of the coastal part of the Asturian basin: Implications for hydrocarbon exploration and for the North-Iberian margin evolution

Hodei Uzkeda [a], Josep Poblet [b,*], Mayte Bulnes [b]

[a] Departamento de Geodinámica, Estratigrafía y Paleontología, Universidad Complutense de Madrid, C/ de José Antonio Novais 12, 28040 Madrid, Spain, EU
[b] Departamento de Geología, Universidad de Oviedo, C/Jesús Arias de Velasco s/n, 33005 Oviedo, Spain, EU

ARTICLE INFO

Keywords:
Asturian basin
Inversion tectonics
Jurassic unconformity
North Iberian margin
vitrinite reflectance

ABSTRACT

The Asturian Basin, situated on the North Iberian margin, is a Permian-Mesozoic extensional basin developed over a Variscan Palaeozoic basement, subsequently inverted during the Cenozoic Alpine orogeny. The compilation of cartographic, structural, biostratigraphic and vitrinite reflectance data collected in a Late Triassic-Jurassic succession, excellently exposed along the Cantabrian Sea coast, has allowed us to gain insight into the Mesozoic and Cenozoic tectono-thermal history of this basin. The oldest recorded event occurred in Middle-Late Jurassic times and consisted of uplift, development of a large syncline, and normal faulting accompanied by circulation of hydrothermal fluids along the faults. The basin emersion caused an angular unconformity, together with a change in the sedimentary environment that passed from marine to continental. A second event, whose age was probably Late Jurassic-Early Cretaceous, was responsible for extensional reactivation of previous normal faults accompanied by a weaker fault-related hydrothermal episode. In Cenozoic (Eocene-Miocene) times, as a consequence of the Alpine orogeny some of the previous faults were reactivated as reverse and/or strike-slip faults, and folds developed. Here we analyse which structures were active during each event, their relationship with the hydrothermal fluids, the control they exerted on the hydrocarbon generation, and how the large-scale models proposed for this portion of the North Iberian margin fit the onshore field observations, in particular regarding the structural position of the Asturian Basin within the Iberian Plate Mesozoic rifts and the role of the Ventaniella Fault.

1. Introduction

The Asturian Basin, situated on the North Iberian margin, is the Mesozoic basin located farthest north on the Iberian Peninsula (Fig. 1). It is a Permian-Mesozoic extensional basin, developed over a Palaeozoic basement deformed during the Variscan orogeny in Carboniferous times, whose early evolution is related to the opening of the Bay of Biscay. Later, during Cenozoic times, the Alpine contractional cycle responsible for the formation of the Cantabrian Mountains and the Pyrenees in the north portion of the Iberian Peninsula caused tectonic inversion of the Asturian Basin.

The Asturian Basin has an emerged part located in the north-northwest portion of the Iberian Peninsula (Fig. 1) and a submerged part beneath the Cantabrian Sea waters. In inland areas, there is considerable vegetation, which results in scattered outcrops, and the best ones are often road and track slopes that provide a 2D view. In the sea, there are a few good quality 3D seismic cubes, old and poor quality 2D seismic lines and some exploration wells (e.g., Zamora et al., 2017). However, both the seismic data and the wells are located several kilometres north of the coast making difficult their correlation with the outcrops on land. The coastal part of the basin probably offers the best prospects for unravelling its structural history because outcrops are generally excellent, and the high coastal cliffs along with platform exposures provide an almost 3D geological view. This is the reason why the coastal area is the main focus of this study, although we will carry out observations throughout the inland portion of the basin. The main drawback of the coastal region is that only part of the stratigraphic succession constituting the basin crops out, primarily consisting of Upper Triassic and Jurassic rocks. In addition, understanding the basin evolution is complicated, unless good 3D outcrops are available, due to

* Corresponding author.
E-mail addresses: huzkeda@ucm.es (H. Uzkeda), jpoblet@uniovi.es (J. Poblet), maite@uniovi.es (M. Bulnes).

https://doi.org/10.1016/j.marpetgeo.2024.107158
Received 11 July 2024; Received in revised form 10 October 2024; Accepted 12 October 2024
Available online 16 October 2024

the points listed below.

i) Faults with different strikes intersect each other (e.g., Julivert et al., 1971; Lepvrier and Martínez García, 1990; Uzkeda, 2013; Uzkeda et al., 2015, 2016; Magán, 2024) making it complex their mapping, specially at the intersection zones.
ii) Many of the faults that compartmentalize this basin were possibly active during various events, either as faults inherited from ancient events that propagated into the Mesozoic cover or as faults formed during Mesozoic extensional events reactivated during the Cenozoic Alpine orogeny (e.g., Lepvrier and Martínez García, 1990; Uzkeda et al., 2012, 2013, 2015, 2016, 2018; Uzkeda, 2013; Magán, 2024).
iii) The presence of faults with various orientations and events of different tectonic nature, led to the development of dip-slip faults (normal, reverse), strike-slip faults (dextral and sinistral), and oblique faults (e.g., Lepvrier and Martínez García, 1990; Uzkeda, 2013; Uzkeda et al., 2015, 2016; Magán, 2024), whose motion is challenging to identify unless accompanied by kinematic indicators and high-resolution stratigraphic information.
iv) Some faults cut and offset folds developed in previous Mesozoic tectonic episodes, giving rise to faults that have both subtractive and additive character along the same fault, and therefore, interpretations of the fault type based on localized observations can be misleading (Magán et al., 2022a, 2022b; Magán, 2024).
v) The length of many faults is relatively small, less than few meters (Magán, 2024), so that unless continuous outcrops are available, it is highly possible that fault traces belonging to different faults may be erroneously mapped as a single fault.

Not many tectonic studies have been carried out in the onshore portion of the basin, however, the completion of various research projects, as well as PhD and MSc theses, in recent years has enabled progress in understanding the structure of selected regions of the emerged part of the Asturian Basin. Taking these premises into account, we have compiled all the available geological maps (e.g., Suárez-Vega, 1974; Merino-Tomé et al., 2023), as well as structural (e.g., Lepvrier and Martínez García, 1990; Alonso López, 2014; Uzkeda, 2013; Odriozola Zubillaga, 2016; Uzkeda et al., 2016; Magán, 2017, 2024), biostratigraphic (e.g., Suárez-Vega, 1974; Goy et al., 2010; Comas-Rengifo et al., 2023) and vitrinite reflectance (e.g., Suárez-Ruiz, 1988; Suárez-Ruiz and González Prado, 1995) data, along with new data collected by ourselves. This has allowed us to achieve three goals. Firstly, propose a tectono-thermal evolution of the emerged part of the basin from Late Triassic-Jurassic to present-day, something never done until now. Secondly, our basin evolution proposal has been examined in terms of the hydrocarbon exploration that various companies carried out in this region in the eighties of past century. Finally, the results obtained have been contrasted with some aspects such as amount of extension or role played by regional-scale faults, which should have been recorded in the Asturian Basin, proposed in large-scale evolution models for the North Iberian margin, with the aim of checking whether they align or not with our conclusions.

2. Geological Setting

The basement of the Asturian Basin is a Palaeozoic succession involved in a fold and thrust belt, named Cantabrian Zone (Fig. 1),

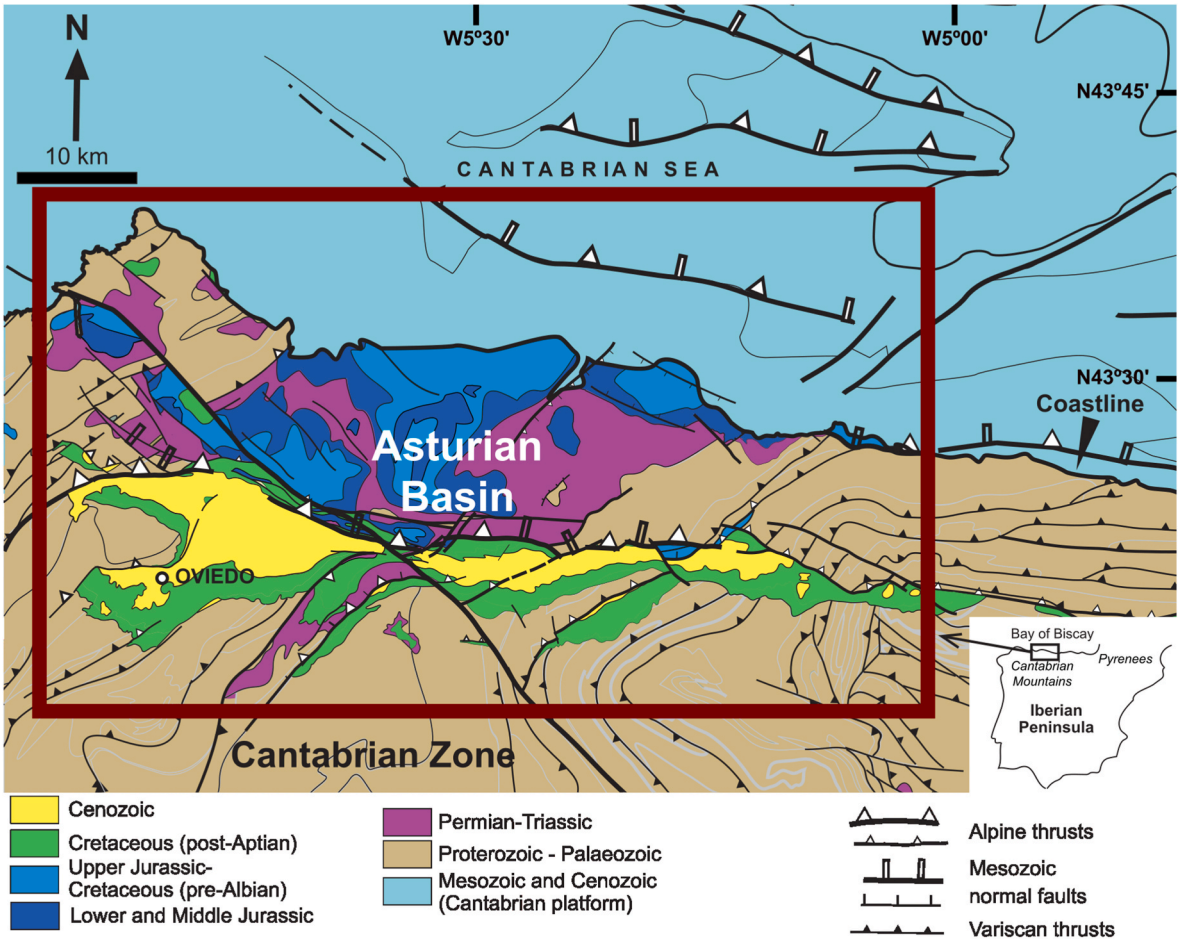

Fig. 1. Simplified geological map of the onshore portion of the Asturian Basin and surrounding regions (modified from Alonso et al., 2009a) and location within the Iberian Peninsula. The red rectangle corresponds to the region illustrated in Fig. 3.

developed during Carboniferous times in the foreland of the Variscan orogen in the north-northwest portion of the Iberian Peninsula (e.g., Lotze, 1945; Julivert et al., 1972a). In cross-sectional view, this belt shows a wedge shape tapering towards the foreland, i.e., towards the east, whereas in map view, it exhibits a curved morphology with the inner core to the east, because it is involved in the Ibero-Armorican or Asturian Arc (e.g., Suess, 1892). The structure of the Cantabrian zone is thin-skinned and it consists of diverse types of thrust systems and fault-related folds (e.g., Julivert, 1971, 1983; Savage, 1979, 1981; Pérez-Estaún et al., 1988; Pérez-Estaún and Bastida, 1990; Aller et al., 2004), strain is limited, and cleavage is only present in some areas. This region developed under diagenetic conditions, and only local parts underwent low to very low-grade metamorphism.

The Asturian Basin (Fig. 1) initiated its development in Permian times, approximately coeval to the onset of the unroofing of the Variscan mountain range westwards of the basin (Grobe et al., 2010). First, as narrow dominantly NE-SW trending isolated basins bounded by inverted Variscan structures (Julivert et al., 1971; Suárez-Rodríguez, 1988; Lepvrier and Martínez-García, 1990; López-Gómez et al., 2019) and later, in Middle-Late Triassic times, as a large compartmentalized basin (López-Gómez et al., 2019). Subsequently, an extensional stage, possibly initiated by the Middle Jurassic (Fernández-López and Suárez-Vega, 1981; Valenzuela et al., 1986, 1989; Lepvrier and Martínez-García, 1990; Uzkeda et al., 2016), caused normal faulting, reactivation of some previous faults, heating, and uplift. This event may have lasted until the lower part of the Early Cretaceous (pre-Barremian) (Alonso et al., 2016; Cadenas and Fernández-Viejo, 2017), although perhaps more than one event occurred from Early Jurassic to Early Cretaceous time. This episode would be related to the opening of the Bay of Biscay located to the north of the Iberian Peninsula.

From the middle-upper part of the Eocene until the beginning of the Miocene (Álvarez-Marrón et al., 1997; Gallastegui, 2000) the convergence between the Iberian and Eurasian tectonic plates caused a contractional event, responsible for selective reactivation of previous structures, as well as the generation of new thrusts and uplifts (e.g., Lepvrier and Martínez-García, 1990; Alonso et al., 1996, 2016; Pulgar et al., 1999; Uzkeda et al., 2016). This event led to the Asturian Basin inversion and formation of the Cantabrian Mountains (Fig. 1) as part of the Alpine orogenic belt. From the upper part of the Eocene to the beginning of the Oligocene, the Alpine structure was exhumed (Fillon et al., 2016). This sequence of events would have been, at least in the offshore part of the basin, influenced by evaporites of Permian-Triassic age that would have acted as a regional detachment (Zamora et al., 2017).

During the Early Pleistocene or even before (e.g., Álvarez-Marrón et al., 2008), the marine abrasion platform, underlain by Cantabrian-Zone Palaeozoic rocks and Asturian-Basin Mesozoic rocks, was eroded, unconformably covered by patches of Quaternary sediments and uplifted above present-day sea level, giving rise to narrow, subhorizontal coastal strips, called marine terraces or "rasas" (e.g., Flor, 1983; Mary, 1983). Additional neotectonic activity, such as development of some new faults and reactivation of some previous ones (e.g., Gutiérrez Claverol et al., 2006; Álvarez-Marrón et al., 2008), as well as small magnitude earthquakes (e.g., López-Fernández et al., 2004), occurred.

3. Methodology and available data

First of all, we have carried out fieldwork to collect new data and map most of the Upper Triassic-Jurassic stratigraphic formations independently, especially in the central and eastern parts of the basin, where some of them were mapped as a single unit in previous geological maps (Julivert and Pello, 1970; Beroiz et al., 1972a, 1972b, 1972c; Julivert et al., 1972b; Martínez-Álvarez et al., 1972; Pignatelli et al., 1972; Suárez-Vega, 1974; Navarro and Rodríguez Fernández, 1984; Alonso et al., 1987–88; Gutiérrez Claverol et al., 2002; Alonso et al., 2016; Merino-Tomé et al., 2023). The main aim of this new geological map is improving our understanding of the structure and geographical distribution of the different stratigraphic units throughout the basin.

Subsequently, several stratigraphic correlation panels, with an approximate E-W orientation along the North-Iberian margin coast covering the whole Asturian Basin from east to west, have been constructed. Their purpose is to help us visualize the large-scale cross-sectional geometry and evolution of the basin at different times using four separate data. One panel has been levelled using Jurassic carbonate horizons below the intra-Jurassic unconformity, another panel has been levelled to the intra-Jurassic unconformity, another panel has been constructed removing the effects of the Cenozoic tectonic structures (both faults and folds), and another has been levelled to the current sea level. These panels have been constructed placing seventeen detailed stratigraphic columns of the Triassic and Jurassic section, with their corresponding biozones taken from Suárez-Vega (1974), Comas-Rengifo and Goy (2010), Comas-Rengifo et al. (2010, 2023), García-Ramos et al. (2010a, 2011), Goy et al. (2010) and Gómez et al. (2016a, 2016b), in their geographical position. Structural data taken from the geological maps referenced above, plus additional data taken from Martín et al. (2013), Uzkeda et al. (2012, 2013, 2015, 2016, 2022), Uzkeda (2013) and own fieldwork, have been added to the stratigraphic correlation panels.

A subcrop map of the intra-Jurassic unconformity throughout the basin has also been constructed using the geological maps listed above, a subcrop map by Julivert et al. (1971), and the biozones identified in different stratigraphic columns. This map shows the distribution of the stratigraphic units below the unconformity, as well as the faults. This subcrop map has been used as the basis for constructing maps of fault activity during each of the tectonic events identified.

To quantify to a certain extent the tectonic activity during each of the different events, the heave and throw of some of the faults mapped in the coastal region have been measured when possible, using average fault dips for each fault. The boundaries between biozones present in both the hangingwall and footwall of the faults have been used as reference surfaces to estimate the measurements.

To decipher the vertical motion of the study area through time employing backstripping, a subsidence curve has been constructed for the Late Triassic-Jurassic succession according to the methodology described in Angevine et al. (1990) and Allen and Allen (2013) amongst others. The ages of the stratigraphic units have been taken from Dubar and Mouterde (1957), Suárez-Vega (1974), Fernández-López and Suárez-Vega, 1981, Olóriz et al. (1988), Barrón et al. (2002, 2006), Schudack and Schudack (2002), Comas-Rengifo and Goy (2010) and Goy et al. (2010), and their numerical values in Ma have been taken from the International Commission on Stratigraphy (2023). The surface porosities, the coefficients that relate porosity and burial depth, and the densities for the different stratigraphic units have been estimated using Sclater and Christie (1980) and Schmoker and Halley (1982) values considering the percentages of different lithologies in the stratigraphic sections of the Jurassic successions constructed by Suárez-Vega (1974) and Valenzuela (1989). The minimum and maximum water depths during sedimentation have been estimated considering the sedimentary environments assigned to each stratigraphic unit by Valenzuela et al. (1986) and García-Ramos and Gutiérrez Claverol (1995). The thicknesses of the stratigraphic units have been taken from the stratigraphic interpretation of the Careñes borehole (Suárez-Vega, 1974). This well has been chosen because of its strategic location in the central-north part of the basin and because the stratigraphic succession intersected in the well is one of the most complete both above and below the intra-Jurassic unconformity.

A graph showing the sea level height versus time, taken from Miller et al. (2020), has been used to unravel the recent evolution of the Asturian Basin. Two functions have been plotted on this graph to illustrate the uplift experienced by the rasa, assuming it emerged at 1 Ma ago and at 2 Ma ago, which are the rasa datings obtained by Álvarez-Marrón

et al. (2008) using cosmogenic nuclides. The plotted functions are linear as they assume that the uplift took place steadily, and these functions reach a height of 150 m above sea level at present-day, which is the current average altitude of the rasa developed on Mesozoic rocks in the central part of the Asturian Basin.

To understand the heat flow distribution within the basin, vitrinite reflectance data from thirty-four outcrops, taken from Suárez-Ruiz (1988), Suárez-Ruiz and González Prado (1995) and Suárez-Ruiz et al. (2006), have been used. The samples are distributed mostly along the coastal cliffs. Most of them (twenty-three) come from the Upper Triassic-Jurassic carbonate sequence below the intra-Jurassic unconformity, whereas the rest (eleven) were taken from the Jurassic detrital sequence above the unconformity. The vitrinite reflectance values have been placed on the stratigraphic columns used to create the stratigraphic correlation panels. Contours of vitrinite reflectance values have been drawn on the correlation panels assuming that they maintain a constant spacing when possible. The aim is to visualize the large-scale thermal pattern of the basin in cross-sectional view.

Two sets of contour maps of vitrinite reflectance values have been constructed to understand the basin thermal pattern in map view. The first set is based on the geographical coordinates and on the reflectance values of the available vitrinite samples interpolated using the algorithm

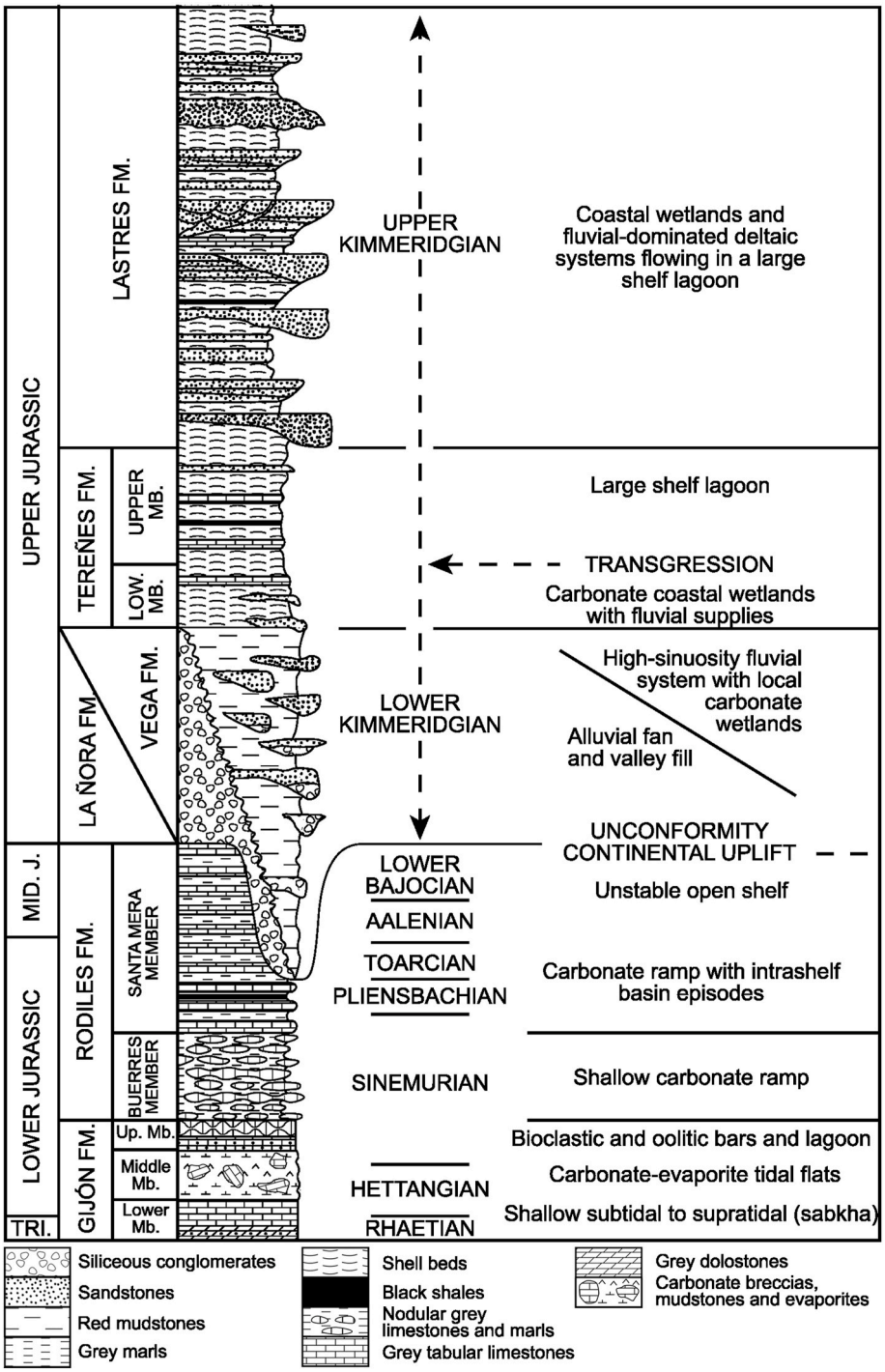

Fig. 2. Stratigraphic section showing the Upper Triassic-Upper Jurassic rocks that crop out in the Asturian Basin (modified from García-Ramos and Gutiérrez Claverol, 1995 based on Valenzuela et al., 1986).

called Triangular Irregular Networks (TIN), implemented in the software QGIS, employing a cell size of 200 x 200 m. This first set of maps assumes that there was no structural control on the heat distribution. The second set of maps of contours of vitrinite reflectance values have been constructed using the geographical coordinates of the samples, their vitrinite reflectance values and the information obtained from the correlation panels. In this second set of maps the activity/presence of faults has a relevant role in the heat distribution.

To determine the paleotemperatures reached during the heating events, the commonly used empirical equations of Barker and Pawlewicz (1994) have been employed to convert all the measured values of vitrinite reflectance to temperatures. The results have been plotted on temperature versus depth graphs, as well as on a temperature versus vitrinite reflectance graph. These authors obtained a coefficient of determination of 0.7, with a mean relative error of around 8%. Thus, in spite of their simplicity (they only considered the reflectance to estimate the temperature and not other variables such as heating time), and errors derived mainly from the difficulty to determine the vitrinite reflectance accurately (Barker and Pawlewicz, 1986) these empirical equations should yield precise enough results for the purpose of our work (Ernst and Ferreiro Mählman, 2004).

4. Stratigraphy

The Upper Triassic-Jurassic rocks that crop out in the coastal portion of the Asturian Basin belong to two sequences separated by an angular unconformity. Both, the main features of the stratigraphic sequences and of the unconformity are described below.

4.1. Stratigraphic succession

The lower sequence, ranging from Rhaetian (Upper Triassic) to lower Bajocian (Middle Jurassic) (Suárez-Vega, 1974; Barrón et al., 2002, 2006), is mainly of carbonate nature and may reach almost 400 m thickness (Fig. 2). The lower part of this sequence, is mainly composed of limestones with some carbonate breccias, dolomites and evaporites, with a thickness of about 200–250 m, and constitute the lower, middle, and upper members of the Gijón Fm. Their approximate ages are Rhaetian, Hettangian and Lower Sinemurian, respectively. This unit was deposited in a sabkha to hypersaline coastal lagoon environment in a tidal flat system, evolving to a bioclastic and oolitic bar-lagoon complex (Valenzuela et al., 1986; Aurell et al., 2002; González-Fernández et al., 2004a; García-Ramos et al., 2006). Its fossil content is scarce, with some lamellibranchs, gastropods and vertebrates. The upper part of the sequence is dominated by alternations of limestones and marls that belong to the Buerres and Santa Mera mbs. of the Rodiles Fm. The lower, Buerres Mb. consists of alternations of grey nodular limestones and less abundant marls, and its thickness is around 60 m. Its age is Upper Sinemurian (Suárez-Vega, 1974; Comas-Rengifo and Goy, 2010; Goy et al., 2010) and it was deposited in a shallow carbonate ramp. Bivalvia, brachiopods and, less frequently, cephalopods may be found in this unit. The upper, Santa Mera Mb., an alternation of grey marls and limestones in similar proportions, from 50 to over 150 m thick, has an age that ranges from Pliensbachian to Lower Bajocian. (Suárez-Vega, 1974; Fernández-López and Suárez-Vega, 1981). It sedimented in a carbonate ramp with intrashelf basin episodes transitioning to an unstable open shelf. This sequence also includes hydrocarbon source rocks, such as bituminous shales and black marls both rich in organic matter of, especially, Pliensbachian and Lower Toarcian age (García-Ramos et al., 1992, 2011; Suárez-Ruiz, 1988; Suárez-Ruiz and González Prado, 1995; Bádenas et al., 2013). Ammonoids are frequent within this unit, as well as lamellibranchs, belemnites and vertebrates (sharks, bony fishes, plesiosaurs and ichthyosaurs). While the lower part of this sequence crops out throughout the Asturian Basin, the upper part crops out mainly in the central-eastern portion of the basin (Fig. 3).

The upper sequence, of Kimmeridgian age (Upper Jurassic) (Dubar

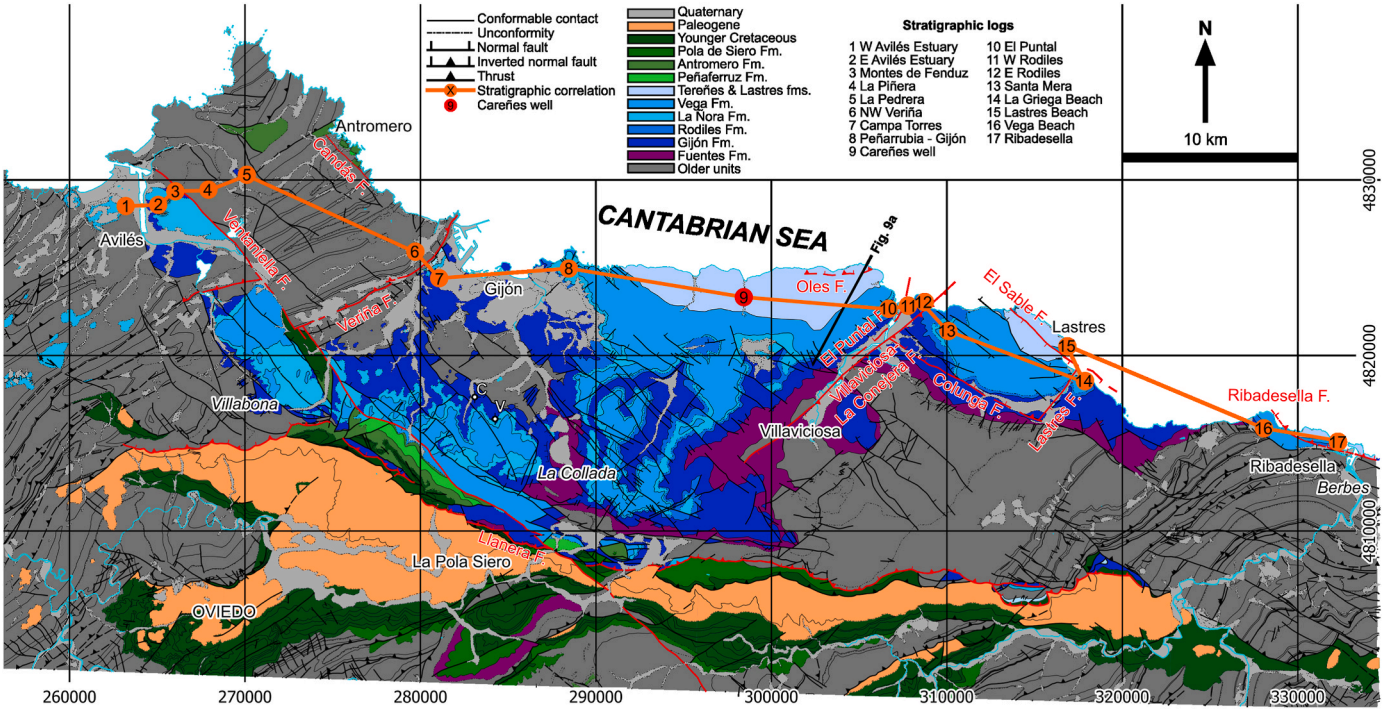

Fig. 3. Geological map of the Upper Triassic-Jurassic rocks that crop out in the emerged portion of the Asturian Basin compiled from data by Julivert and Pello (1970), Beroiz et al. (1972a, 1972b, 1972c), Julivert et al. (1972b), Martínez-Álvarez et al. (1972), Pignatelli et al. (1972), Suárez-Vega (1974), Navarro and Rodríguez Fernández (1984), Alonso et al. (1987–88), Uzkeda (2013), González-Fernández et al. (2014), Alonso et al. (2016), Merino-Tomé et al. (2023) and own data. The faults mentioned in the text are shown in red. The mining districts (Villabona, La Collada and Berbes) are shown in italics. V: Vilorteo well. C: Cantavieyo well. The location of the stratigraphic logs illustrated in Figs. 4, 5 and 12, and the location of the geological cross-section depicted in Fig. 9a, are shown. See Fig. 1 for location.

and Mouterde, 1957; Olóriz et al., 1988; Schudack and Schudack, 2002), is mainly of detrital nature and its thickness may reach almost 450 m (Fig. 2). It consists of a lower part made up of conglomerates, sandstones and red mudstones that belong to La Ñora and Vega fms., which are lateral equivalents and show thicknesses of up to 150 m. The former corresponds to alluvial fans that progressively pass to the high-sinuosity fluvial systems with local carbonate wetlands characteristics of the latter. The fossil content, less abundant than in the underlying unit, is composed of plants, vertebrates (fishes, dinosaurs, and other reptiles mainly) and ichnofossils of both invertebrates and vertebrates. The siliciclastic facies tend to appear in meter-scale fining-upward sequences. The conglomerates are well cemented and formed by siliceous, rounded clasts of 3–12 cm, embedded in a sandy matrix (García-Ramos et al., 1979). The most frequent sedimentary structures found in the sandstones are epsilon, tabular and trough cross bedding, together with bioturbation (García-Ramos et al., 1979). The mudstones deposited between the channels show evidences of an arid environment, such as rhizoconcretions, mudcracks and caliche deposits (García-Ramos et al., 1979; Valenzuela et al., 1986). The middle part of the sequence is formed by marls and some interbedded limestone and sandstone levels which constitute the Tereñes Fm. Its thickness oscillates between 60 and 160 m, mainly because of its transition to the overlying unit. The Tereñes Fm. was deposited in carbonate coastal wetlands with fluvial courses draining to a shelf lagoon separated from the open ocean by a threshold or barrier that prevented the entry of stenohaline fauna (García-Ramos et al., 2010b; Fürsich et al., 2012). Plant remains are frequent, as well as gastropods, lamellibranchs (forming shell beds) and vertebrates (sharks, bony fishes, turtles, plesiosaurs, crocodiles, and pterosaurs) and dinosaur tracks. The upper part of the sequence is mainly made up of sandstones, shales, and marls, with occasional conglomerates, which belong to the Lastres Fm. The total preserved thickness of the Lastres and Tereñes fms. is about 300 m. The conglomerates and sandstones were deposited by fluvial-dominated deltaic systems prograding on the lagoon represented by the marls of the Tereñes Fm.

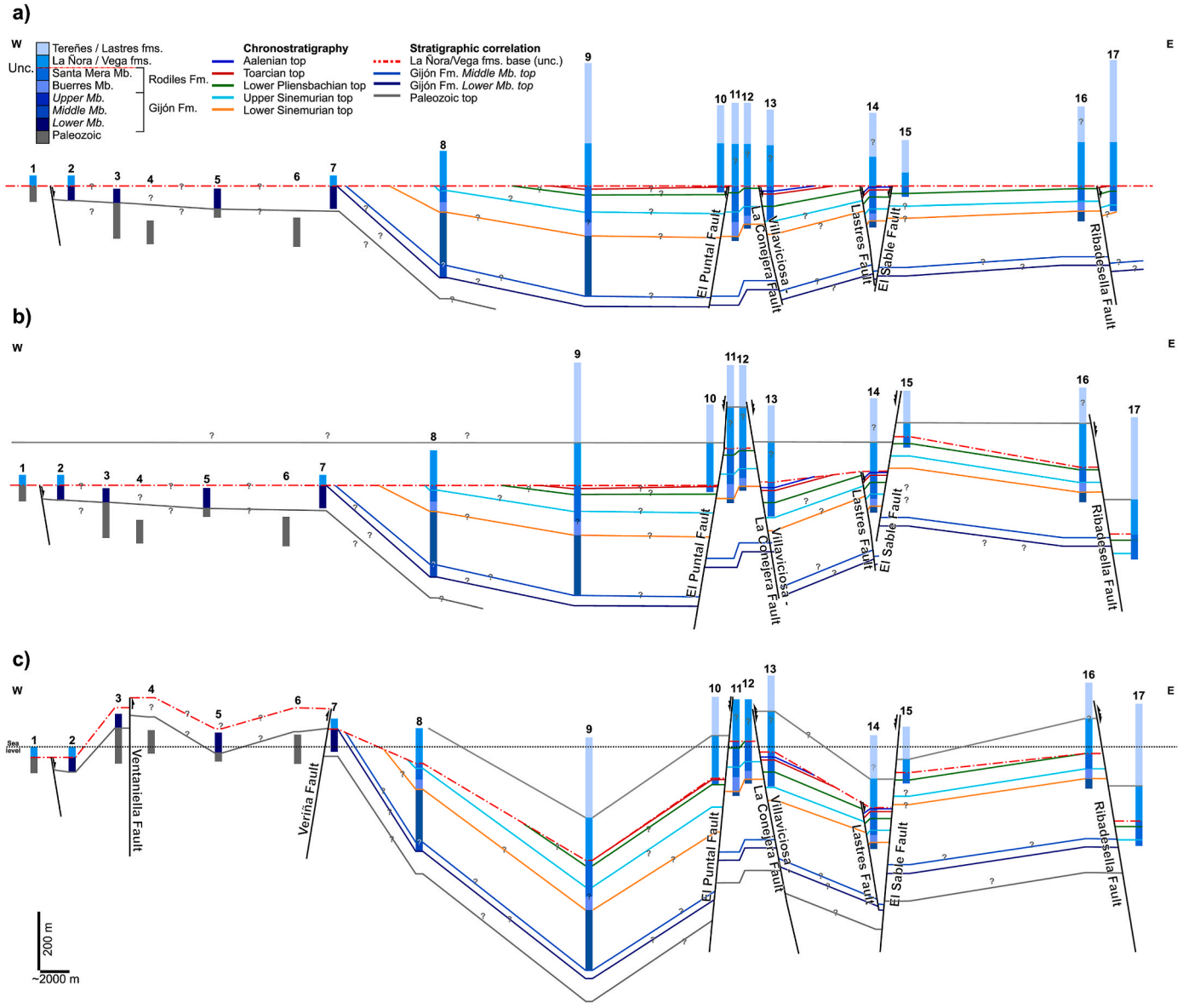

Fig. 4. Stratigraphic correlation panels of the Upper Triassic-Jurassic rocks that crop out in the coastal part of the Asturian Basin. a) Panel levelled to the intra-Jurassic unconformity, b) panel constructed by removing the effect of the Cenozoic faults presented in Table 1 as well as the folds, and c) panel levelled to the present-day sea level. These figures have been created using biostratigraphic and structural data from Suárez-Vega (1974), Comas-Rengifo and Goy (2010), Comas-Rengifo et al. (2010, 2023), García-Ramos et al. (2010a, 2011), Goy et al. (2010) Martín et al. (2013), Uzkeda et al. (2012, 2013, 2015, 2016, 2022), Uzkeda (2013), Gómez et al. (2016a, 2016b) and own data. The vertical scale of the panels is exaggerated (~20x). See location of stratigraphic logs in Fig. 3.

The clasts of the conglomerates tend to be smaller (typically less than 5 cm) than in La Ñora and Vega fms., and the sandstones have calcareous cement and, commonly, cross bedding. The Lastres Fm. fossils are similar to those of the Tereñes Fm., adding the presence of dinosaur body remains and pterosaur tracks. Again, this sequence includes some organic matter-bearing black marls and shales interbedded within the grey marls of the Tereñes and Lastres fms. (Valenzuela et al., 1986; Valenzuela, 1989). While the lower part of this sequence crops out throughout the Asturian Basin, the middle and upper parts crop out mainly in the north central-eastern portion of the basin (Fig. 3).

4.2. The intra-Jurassic unconformity

The intra-Jurassic unconformity (Fig. 2), which represents an important sequence boundary (Catuneanu et al., 2010), is an angular unconformity (e.g., Almela and Rios, 1962; Suárez-Vega, 1974; Magán, 2024), so that the strata located above the unconformity are slightly oblique to the strata located below. La Ñora and Vega Jurassic fms. lie always above the unconformity, however, different rocks appear beneath the unconformity. In the western part of the Asturian Basin, the unconformity truncates progressively older stratigraphic units towards the west (Fig. 4a): the two members of the Rodiles Fm., the three members of the Gijón Fm. and finally Triassic-Palaeozoic rocks in the western edge of the basin. Neither the Rodiles Fm. nor the Gijón Fm. exhibit facies variations or thin out westwards, in fact, the lower Pliensbachian and upper Sinemurian rocks, whose thickness is relatively well constrained using biozones, thicken to the west. These observations confirm that the disappearance of these stratigraphic units below the unconformity is due to the erosion associated with the angular unconformity and rule out the possibility that their disappearance could be attributed to a basin boundary (García-Ramos, pers. com.). Offshore to the northeast of the Asturian Basin, an intra-Jurassic unconformity was proposed by Boillot et al. (1979) around the Le Danois Bank area, where Kimmeridgian-Portlandian limestones would lie unconformably on top of older Jurassic units in a downthrown fault block and on the pre-Mesozoic basement in the uplifted fault block.

The unconformity results in no record of rocks belonging to the upper part of the Middle Jurassic and to the lower part of the Upper Jurassic. Thus, the age of the youngest rocks situated beneath the unconformity is Bajocian (e.g., Suárez-Vega, 1974), while the age of the rocks located above the unconformity is Kimmeridgian (e.g., Dubar and Mouterde, 1957) (Fig. 2). Between the Bajocian top (168.2 ± 1.2 Ma) and the Kimmerigdian base (154.8 ± 0.8 Ma) there is a time gap of 13.4 ± 2 Ma that comprises the Bathonian and Callovian (upper part of the Middle Jurassic), and the Oxfordian (lower part of the Late Jurassic). The ages in Ma have been taken from the International Commission on Stratigraphy (2023).

A significant change in the sedimentary environment between the rocks located below and above the unconformity occurs. While the youngest rocks below the unconformity, belonging to the Rodiles Fm., were deposited in a shallow marine environment (open shelf) (e.g., Valenzuela et al., 1986; García-Ramos and Gutiérrez Claverol, 1995), the stratigraphic units above the unconformity, i.e., La Ñora and Vega fms., are of continental origin (alluvial fan and fluvial) (e.g., Valenzuela et al., 1986; García-Ramos and Gutiérrez Claverol, 1995) (Fig. 2). The transition from marine facies below the unconformity to continental facies above the unconformity took place during the Jurassic, a period that experimented a global sea level rise (e.g., Hallam, 2001). This might suggest that this sequence boundary was mainly the result of a tectonic process, which could be analogous to that described for the North Sea (e.g., Underhill and Partington, 1993; Davies et al., 1999), rather than controlled by eustasy. However, from Bajocian to Kimmeridgian time several sea level drops occurred (Haq et al., 1987; Hardenbol et al., 1998; Haq, 2018) and, consequently, the youngest of them before the La Ñora and Vega fms. deposition could have also left its imprint.

To gain insight into the origin of the unconformity, we have first considered that the rocks beneath the unconformity had an approximately flat-lying attitude before the unconformity (Fig. 5). In this case, the truncation of different stratigraphic units by the unconformity should be interpreted as a result of ancient paleoreliefs, so that the unconformity would exhibit a markedly non-planar geometry. In this scenario, it is likely that La Ñora and Vega fms. layers above the unconformity would display onlap situations where the unconformity is more inclined. However, such situations have not been observed in the field. Furthermore, the unconformity would have an approximately convex geometry at large-scale with a depressed western portion of the basin and a raised region in the central and eastern portions of the basin. However, the central and eastern portions of the basin are currently sunken with respect to the western portion, as shown in Fig. 4c. Therefore, this scenario, which attributes a paleorelief origin to the intra-Jurassic unconformity, does not seem to align well with the observations made in the field. Thus, all the arguments presented above indicate that the disappearance of the Rodiles and Gijón fms. beneath the unconformity did not result from paleoreliefs, basin boundaries and/or eustatic processes. An alternative hypothesis to explain the origin of the unconformity assumes that the rocks beneath the unconformity were affected by tectonic structures prior to erosion, in such a way that the unconformity would truncate both different stratigraphic units and structures (Fig. 4a). This scenario seems appropriate as it is in accordance with the observations made. The tectonic structures developed before the unconformity are described in the next section.

5. Tectonics

The analysis presented below primarily takes into account the major structures that crop out along an E-W section along the coastal area.

5.1. Mesozoic faults and folds active before the intra-Jurassic unconformity

In an E-W cross-sectional view along the coast, the overall structure of the Asturian Basin at the time of development of the intra-Jurassic unconformity was, in broad terms, a very open, large syncline spanning tens of kilometres (Fig. 4a). This fold was asymmetric since its western E-dipping limb was more inclined than its eastern, W-dipping limb. There is no evidence of growth strata related to the syncline amplification since bed thickness is approximately constant except for some Rodiles Fm. biozones that thin slightly eastwards. Thus, this syncline developed after the deposition of the youngest sediments located beneath the unconformity and prior to the unconformity as the syncline is truncated by the unconformity.

In the coastal part of the Asturian Basin, some normal faults with NE-SW strike dipping both to the NW and SE (El Puntal, Villaviciosa-La Conejera, Lastres), faults with NW-SE strike dipping to the SE (El Sable), and faults with E-W to NW-SE strike dipping to the N (Ribadesella) were active before development of the intra-Jurassic unconformity (Fig. 4a and 6a). Estimated normal throws along these faults range between approximately 11 m and 50 m, while heaves vary approximately from 6 to 29 m (Table 1). The faults with the largest throws are those that strike NE-SW (Villaviciosa-La Conejera and Lastres) (Table 1). El Puntal Fault and the Villaviciosa-La Conejera Fault delimit a narrow horst located at the core of the syncline described above, the Lastres Fault and El Sable Fault bound a narrow graben in the eastern syncline limb, and El Sable and the Ribadesella Fault bound a wide horst eastwards (Fig. 4a). The fault activity map (Fig. 6a) and the unconformity subcrop map (Fig. 7) of the whole basin show that the faults active during this event had a predominant NW-SE strike and that there is a large number of faults developed throughout the basin. No evidence of growth strata related to fault development have been identified, as the thicknesses of the pre-unconformity layers identified in the hangingwalls and footwalls of the faults are approximately identical. The Rodiles Fm. biozones preserved in the hangingwalls and footwalls of

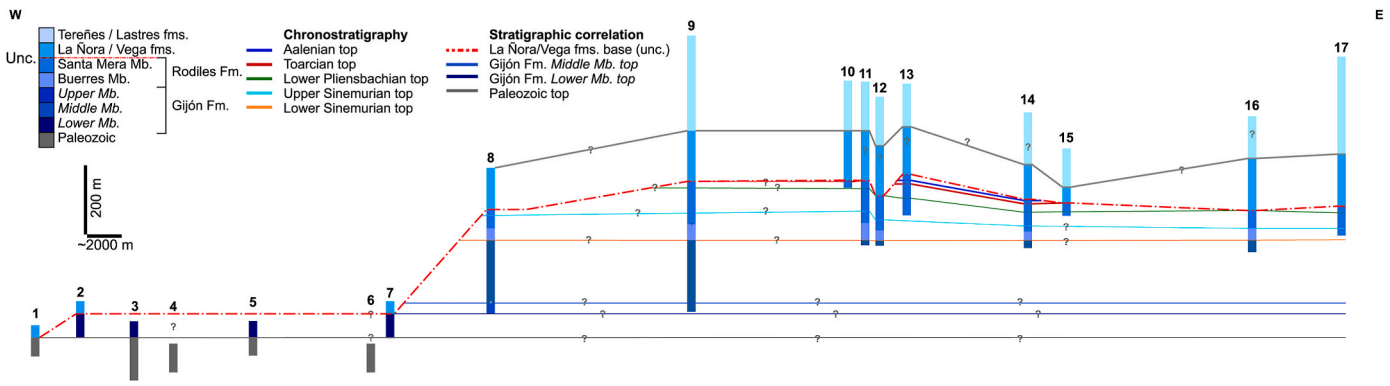

Fig. 5. Stratigraphic correlation panel of the Upper Triassic-Jurassic rocks that crop out in the coastal part of the Asturian Basin levelled to the Rodiles Fm. biozones. The data used to construct this correlation panel are the same than those used to construct the correlation panels illustrated in Fig. 4. The vertical scale of the panel is exaggerated (~20x). See location of stratigraphic logs in Fig. 3.

these faults are different because both successions, as well as the faults, are truncated by the intra-Jurassic unconformity. Therefore, the activity of these faults occurred after the youngest Rodiles Fm. biozone and before the intra-Jurassic unconformity. Had these faults generated depocenters, the corresponding growth strata would have been completely removed by the subsequent erosion.

In summary, between the middle part of the Middle Jurassic and the lower part of the Late Jurassic the basin acquired a synclinal geometry and several normal faults with various orientations were active.

5.2. *Mesozoic faults active after the intra-Jurassic unconformity*

Nowadays, some normal faults cut and offset all the Jurassic stratigraphic units including the intra-Jurassic unconformity and their normal throw is greater than the one they had during the event preceding the intra-Jurassic unconformity. This situation is interpreted as a normal reactivation of these pre-unconformity normal faults. In the coastal part of the basin, the reactivated faults strike NE-SW (El Puntal, Villaviciosa-La Conejera), NW-SE (El Sable), and E-W to NW-SE (Ribadesella) (Fig. 4b and 6b). Estimated normal throws along these faults range from 68 m to 209 m, while heaves vary between 32 and 97 m (Table 1). The largest throws occur along faults whose strikes are E-W to NW-SE (Ribadesella) and NW-SE (El Sable) (Table 1). Both the horst at the hinge of the syncline described above and the graben in its eastern limb are accentuated due to the increased normal displacement along the faults that bound them. As a result, the geometry of the central-eastern part of the syncline is disrupted (Fig. 4b). According to the fault activity map of the whole basin (Fig. 6b), the faults active during this time usually exhibit a NW-SE strike, the number of active faults is moderate, and they seem to concentrate in the central part of the basin. These observations must be taken with caution as they may be biased by the outcrop distribution of the post-unconformity units (Fig. 3). The age of these faults is assumed to be Mesozoic as explained below.

A few normal faults developed in the Asturian Basin after the intra-Jurassic unconformity have been dated. These faults have provided ages ranging from the middle part of the Late Jurassic to the middle part of the Early Cretaceous. The first dated fault corresponds to an E-W decametre-scale fault developed during the Vega Fm. sedimentation, i.e., Kimmeridgian (Late Jurassic). This fault exhibits a syn-sedimentary breccia formed by sandstone blocks, local concentrations of oncoids, and a small paleochannel filled in with sandstone and breccia whose orientation is very different from that of the contemporaneous river network (García-Ramos et al., 2010c; Uzkeda, 2013; Uzkeda et al., 2016). The second and third faults, somewhat larger in size than the previous one, correspond to NW-SE faults synchronous with the Tereñes Fm. sedimentation, also of Kimmeridgian age (Late Jurassic). One of these faults shows detrital beds in the fault hangingwall absent in the footwall, while the other fault (El Sable Fault) displays a somewhat thicker succession in the hangingwall compared to that in the footwall (Uzkeda, 2013; Uzkeda et al., 2016). This fault may have also been active during the Vega Fm. sedimentation since this formation seems to be thicker in the downthrown block. The fourth fault, an E-W kilometre-scale fault, larger in size than the previous ones, was active from the Late Jurassic to the pre-Barremian Early Cretaceous. The age of the rocks involved in the fault, along with pollen dating at the base of the sequence deposited after the fault, allowed its age to be constrained (Alonso et al., 2009a, 2016). Thus, according to the ages provided by the four faults described above, the post-unconformity normal motion of El Puntal, Villaviciosa-La Conejera, El Sable, and Ribadesella faults might have been produced between the Late Jurassic and the pre-Barremian Early Cretaceous.

In summary, from the Late Jurassic to the pre-Barremian Early Cretaceous, many normal faults active during the pre-unconformity event were reactivated as normal faults.

5.3. *Faults and folds active during Cenozoic times*

Nowadays, some faults that cut and offset the Jurassic succession exhibit reverse motion (Ventaniella, Veriña), while others display normal motion but acted as reverse faults because they exhibit evidence of buttressing (Villaviciosa-La Conejera, Ribadesella) (Alonso et al., 2009a; Uzkeda, 2013; Uzkeda et al., 2012, 2013, 2015, 2016, 2022; Martín et al., 2013). In the coastal part of the Asturian Basin these faults strike NE-SW (Veriña, Villaviciosa-La Conejera), NW-SE (Ventaniella), and E-W to NW-SE (Ribadesella) (Fig. 4c and 6c). Estimated reverse throws along these faults range between 50 m and 80 m, while heaves vary from 37 to 70 m (Table 1). The NE-SW faults (Veriña and Villaviciosa-La Conejera) are the ones that exhibit the largest throws (Table 1). The fault activity map of the whole basin (Fig. 6c) shows that the predominant strike of faults active during this event is variable, their number is rather limited, and they are mainly concentrated in the southern part of the basin. The age of these faults is assumed to be Cenozoic, given that reverse and strike-slip faults with NE-SW, NW-SE, and E-W strikes cutting and offsetting Paleogene-Neogene rocks have been mapped in many geological maps of this region (Beroiz et al., 1972a, 1972b; Martínez-Álvarez, 1972; Merino-Tomé et al., 2023 amongst others).

The coastal part of the Asturian Basin is made up of several slightly asymmetric anticlines and synclines of kilometric dimensions, so that the western limbs of the synclines have a greater dip than the eastern limbs giving them a faint eastern vergence. The syncline and adjacent anticlines located between the Ventaniella Fault and the Veriña Fault in the western part of the basin might correspond to a Cenozoic pop-up structure related to the reverse motion of both faults (Fig. 4c). The

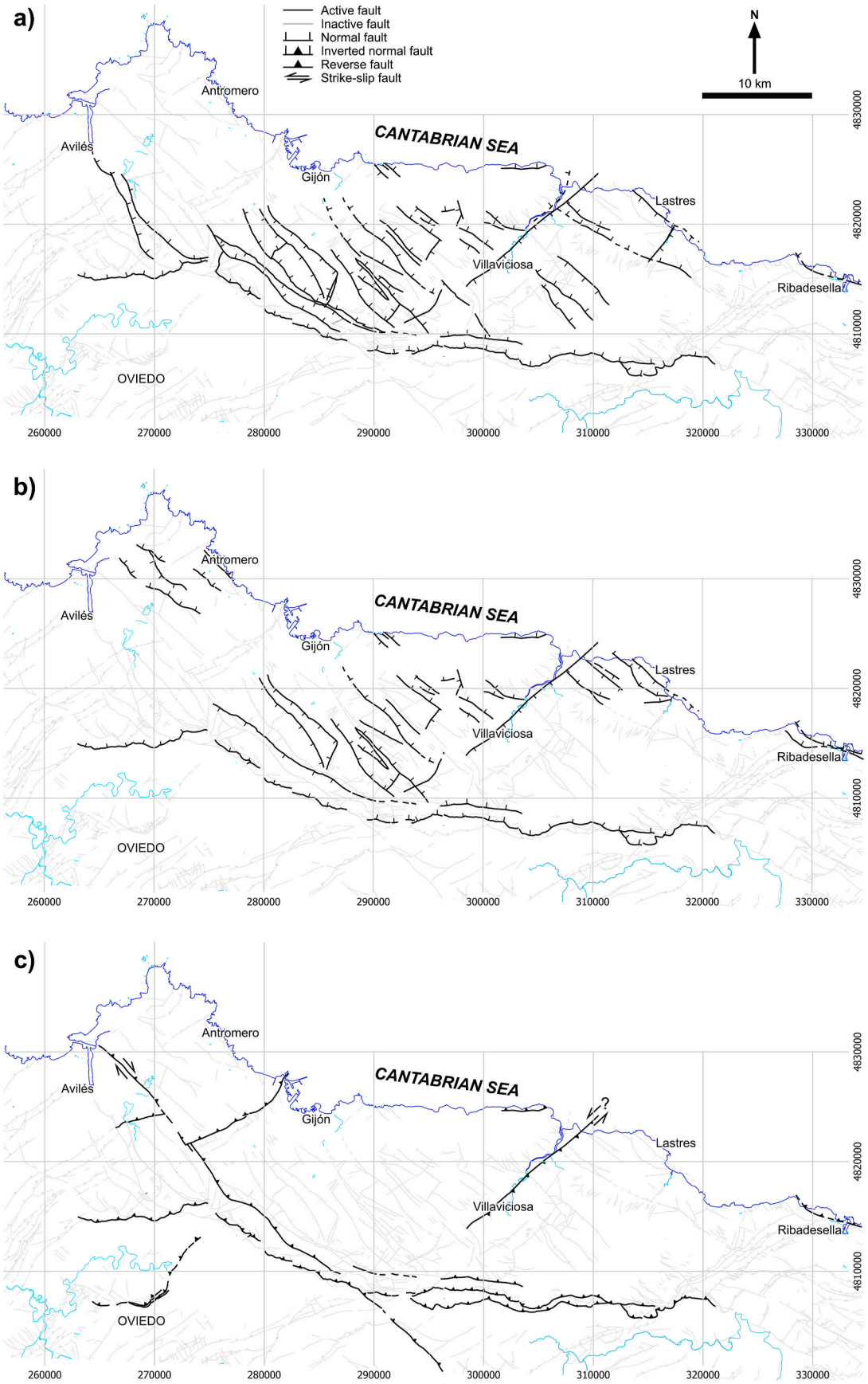

Fig. 6. Structural sketches showing: a) Mesozoic normal faults active before the intra-Jurassic unconformity, b) Mesozoic normal faults active after the intra-Jurassic unconformity, and c) reverse faults active during the Cenozoic.

Table 1
Values of throw and heave for the faults displayed in Fig. 4 during the pre-unconformity extensional stage (Pre-Unc), the post-unconformity extensional stage (Post-Unc), the contractional stage (Alpine) and nowadays (Current). The Villaviciosa-La Conejera Fault values have been obtained from Uzkeda et al. (2013). Positive values: normal displacement; negative values: reverse displacement.

FAULT	DIP	Throw				Heave			
		Pre-Unc	Post-Unc	Alpine	*Current*	Pre-Unc	Post-Unc	Alpine	*Current*
Ventaniella	90			−50	−50			?	?
Veriña	45			−70	−70			−70	−70
El Puntal	60	11	120		131	6	69		76
Villaviciosa-La Conejera	65	50	68	−80	38	23	32	−37	18
Lastres	60	50			50	29			29
El Sable	60	12	168		180	7	97		104
Ribadesella	75	22	209	?	231	6	56	?	62

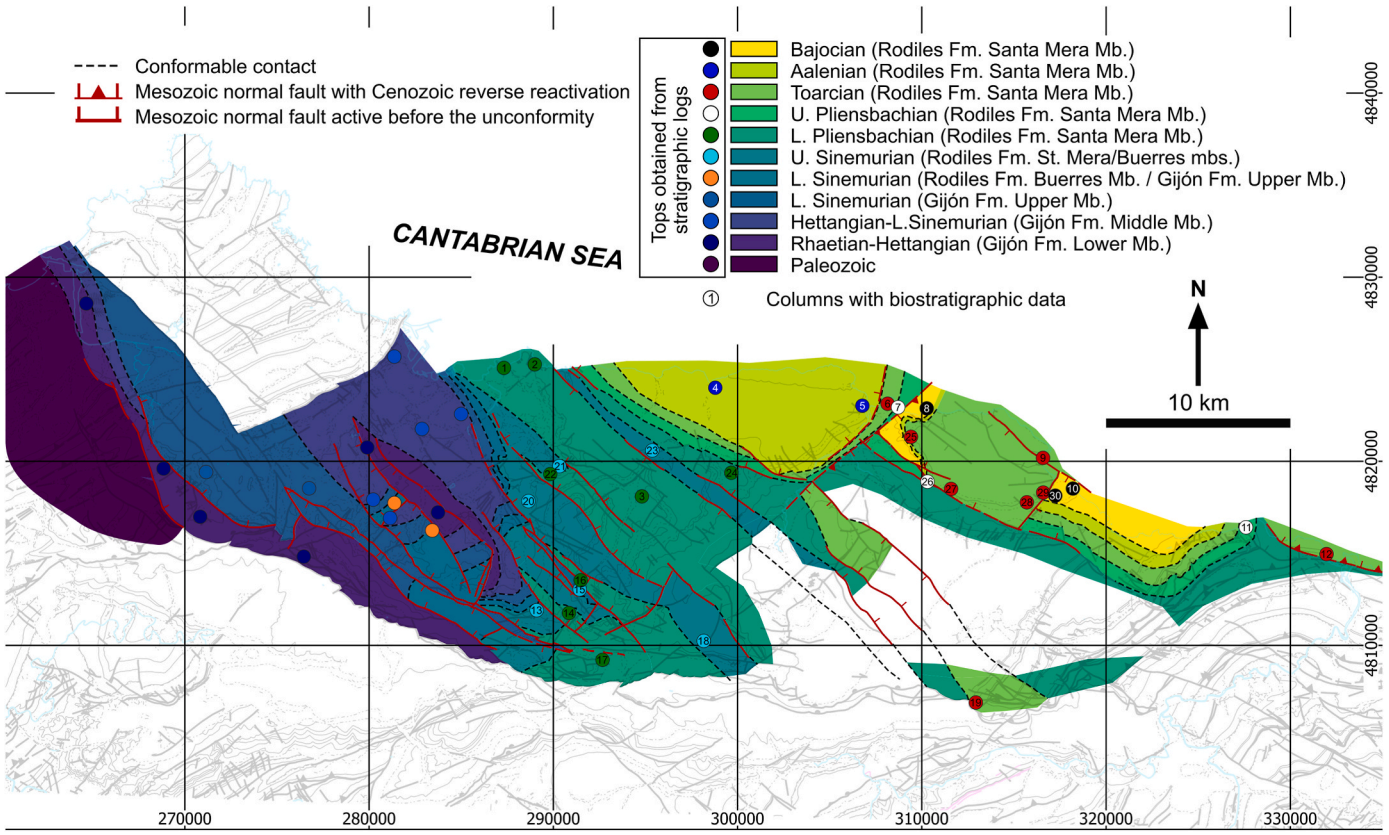

Fig. 7. Subcrop map of the intra-Jurassic unconformity under La Ñora and Vega fms. Active faults during different tectonic events are also shown. This map is based on the maps used to construct the geological map in Fig. 3 and on the biostratigraphic data presented in Table 2.

anticline located at the central part of the basin possibly nucleated from the disturbance caused by the horst bounded by El Puntal and the Villaviciosa-La Conejera faults, as this horst is situated at the anticline hinge (Fig. 4c). Similarly, the syncline located in the eastern part of the basin may have nucleated from the graben located at its core, bounded by the Lastres Fault and El Sable Fault (Fig. 4c).

With respect to neotectonic activity, earthquakes along the Ventaniella Fault (e.g., López-Fernández et al., 2018; Fernández-Viejo et al., 2021), submarine landslides close to the fault (Fernández-Viejo et al., 2014), and the fact that its trace is located in between two portions of the Quaternary coastal rasa with different elevations (López-Fernández et al., 2020) evidence its Quaternary activity. Concerning the Veriña Fault, in the study area, the uplifted fault block, primarily formed by Cambrian-Ordovician quartzites, is approximately 160 m above the sunken fault block, consisting of Permian-Triassic-Jurassic detrital, carbonate, and evaporitic rocks (e.g., Beroiz et al., 1972c; Magán, 2024). This significant elevation difference between the fault hangingwall and footwall could simply evidence distinct erosion resistance of the rocks in both fault blocks, however, it may also be interpreted as a potential outcome of recent tectonic activity.

In summary, during the Paleogene-Neogene, faults with various orientations were active and new folds developed, whereas during the Quaternary a few faults remained active.

5.4. Fault reactivations

Considering the number of reactivations suffered by the main faults that crop out along the coastal part of the Asturian Basin, three types of faults can be distinguished (Fig. 4): i) faults that moved only once, either as normal faults (Lastres, NE-SW strike, SE dip) or as reverse faults (Ventaniella (NW-SE strike, near vertical dip), Veriña (NE-SW strike, NW dip)), ii) faults that moved twice as normal faults (El Puntal (NE-SW strike, NW dip), El Sable (NW-SE strike, SW dip)), and iii) faults that moved three times, twice as normal faults and once as reverse faults

(Villaviciosa-La Conejera (NE-SW strike, SE dip), Ribadesella (WNW-ESE strike, NNE dip)). Faults active during only one of the two extensional events and subsequently during the contractional event have not been recognized. However, these results should be taken with caution, because of the reasons explained below. i) There might have been reactivations involving movements below the resolution of our working method. ii) There might be faults that currently exhibit a normal offset, but nonetheless, they could have experienced reverse reactivation in a way that the overall motion balance remained normal, i.e., they did not reach the null point. Without evidence such as buttressing, etc., we would not have been able to detect their reactivation. iii) Similarly, faults that currently display reverse motion could have been normal in the past. However, if the inversion managed to exceed the entire normal movement, we would not have been able to decipher their activity as normal faults unless there were pieces of evidence such as buttressing, biostratigraphic differences, etc. Fault reactivation was selective, but there is no correlation between the number of times the faults have been reactivated, their trend and their geographical position. Regarding the amount of motion that took place during each event, in the case of faults that were active during the two extensional events, the amount of fault motion was higher during the younger extensional event, ranging approximately between 1.4 and 14 times (Table 1).

Regarding the origin of the faults, the NE-SW trending faults (Veriña, El Puntal, Villaviciosa-La Conejera, Lastres) might be reverse faults developed in the Palaeozoic rocks that make up the Asturian Basin basement later on propagated across the basin cover during Mesozoic and/or Cenozoic times. The Variscan structures exhibit a NE-SW trend in this area (e.g., Julivert and Pello, 1970; Alonso et al., 1987–88) because the Asturian Basin is located above the northern branch of the Ibero-Armorican or Asturian arc (e.g., Pérez-Estaún et al., 1988; Pérez-Estaún and Bastida, 1990; Aller et al., 2004) (Figs. 1 and 3). If this was correct, perhaps some of the faults described above might be inherited faults, so that some faults classified as active during only one event might have been active during two events (Veriña, Lastres), others classified as active during two events might have been active during three events (El Puntal), and others active during three events might have been active during four events (Villaviciosa-La Conejera, which might correspond to the negative inversion of the Pajares Fault/Back-thrust (Aller, 1986; Alonso et al., 2009b)). In addition, some authors describe the existence of NE-SW and NW-SE striking faults active during Permian and Triassic times (Julivert et al., 1971; Sánchez de la Torre et al., 1977; Suárez-Rodríguez, 1988; Lepvrier and Martínez-García, 1990; López-Gómez et al., 2019). Thus, some of the faults described above could have experienced a multiple event activity.

5.5. Late Triassic to present-day tectonic subsidence/uplift

During the sedimentation of the carbonate succession (Gijón Fm., and Buerres and Santa Mera mbs. belonging to the Rodiles Fm.) from the upper part of the Late Triassic to the middle part of the Middle Jurassic, tectonic subsidence at a moderate, and approximately constant rate of 20 m/Ma occurred (Fig. 8). In contrast the sedimentation rate slowed down, passing from around 16 m/Ma during the Gijón Fm. deposition to about 5 m/Ma for the Buerres and Santa Mera mbs. (Rodiles Fm.).

Three observations point out an uplift of the western portion of the Asturian Basin, extending farther westward, together with erosion: i) the disappearance of the Gijón and Rodiles fms. beneath the intra-Jurassic unconformity towards the west (Figs. 3 and 4a), ii) the facies geographical distribution within La Ñora and Vega fms. with proximal coarse facies in the west and distal finer facies in the east (Valenzuela, 1989; García-Ramos et al., 1979; Sánchez de la Torre and Barba Regidor, 1981), and iii) the composition of conglomerate clasts in La Ñora Fm. whose main source area are Palaeozoic units situated farther west (García-Ramos, pers. com.) exhumed from Triassic to Late Jurassic (Grobe et al., 2010). This uplift occurred after the sedimentation of the Gijón and Rodiles fms. (middle part of the Middle Jurassic) because, as mentioned above, their thickness and facies remain constant, but before the development of the unconformity (lower part of the Late Jurassic) as they are truncated by the unconformity. It remains uncertain whether this uplift continued during the sedimentation of La Ñora and Vega fms.; thus, the facies distribution and the provenance of the conglomerates within these two formations might be diagnostic of deposition coeval to uplift, but they might also be interpreted as a result of an inherited paleorelief responsible for a paleodepositional slope. This rapid basin uplift (40 m/Ma) took place at a faster rate than the previous tectonic subsidence (Fig. 8).

Once tectonic subsidence resumed during the middle part of the Upper Jurassic, detrital sedimentation resumed as well. During the sedimentation of La Ñora and Vega fms., tectonic subsidence occurred at a moderate rate of 25 m/Ma, slightly greater than that which occurred during the sedimentation of the Jurassic carbonate succession. However, soon the tectonic subsidence rate increased considerably to high values of 70 m/Ma during the sedimentation of the Tereñes and Lastres fms. (Fig. 8).

The subhorizontal strip of land developed above the coastal portion of Asturian Basin called rasa, elongated in an E-W direction approximately parallel to the coast, with a height of tens of meters above sea level, bounded to the north by a cliff over the Cantabrian Sea and to the south by the Cantabrian Mountains (Fig. 9a), and interpreted as a marine abrasion platform nowadays elevated above sea level (e.g., Álvarez-Marrón et al., 2008; López-Fernández et al., 2020), is a testimony of a relatively recent emersion suffered by this part of the Asturian Basin. The combination of multiple cosmogenic nuclides gave a minimum age of 1–2 Ma, i.e., Early Pleistocene (lower part of the Quaternary), for the rasa located to the west of the studied area, whose height increases progressively from west to east reaching heights of approximately 100 m above sea level to the east of the Asturian Basin (Álvarez-Marrón et al., 2008). In the study area the rasa reaches average altitudes of 150 m above sea level (Fig. 9a). Assuming that the age of the rasa in the study area is the same as that estimated by Álvarez-Marrón et al. (2008), Fig. 9b shows that the current position of the rasa was not due to a sea level drop, but to a land uplift. Assuming that this uplift occurred at a constant rate, it took place at a very fast rate of approximately 92–194 m/Ma, or equivalently, 0.09–0.19 mm/year.

6. Thermal Regime

The vitrinite reflectance values obtained in the Upper Triassic-Jurassic carbonate rocks plotted on a map and contoured show two maxima: one maximum just south of a locality called Lastres (1.53) in the central-eastern part of the basin and a second one, less intense, around a locality called Ribadesella (1.27) in the easternmost edge of the basin (Table 3, Fig. 10a). The vitrinite reflectance values collected from the Jurassic detrital rocks plotted on a map and contoured exhibit only one maximum (1.24) in the surroundings of Ribadesella (Table 3, Fig. 10b), i.e., close to the 1.27 maximum shown by the underlying rocks. Where the lower sequence displays its maximum value (1.53), there is no local maximum in the upper sequence which displays a relatively small value (0.52) instead. The discrepancy between the position of the maxima in the lower and upper successions suggest that there may have been at least two different main heating events: an old one developed after the deposition of the lower carbonate succession but before the detrital succession deposition, i.e., before the intra-Jurassic unconformity, and a younger one developed after the deposition of the upper detrital succession affecting the whole Jurassic succession, i.e. after the intra-Jurassic unconformity.

6.1. Heating event developed before the intra-Jurassic unconformity

The vitrinite reflectance values recorded in the lower carbonate succession for this event range from less than 0.50 to 1.53 (Table 3), and they increase from west to east when contoured on a map (Fig. 10a).

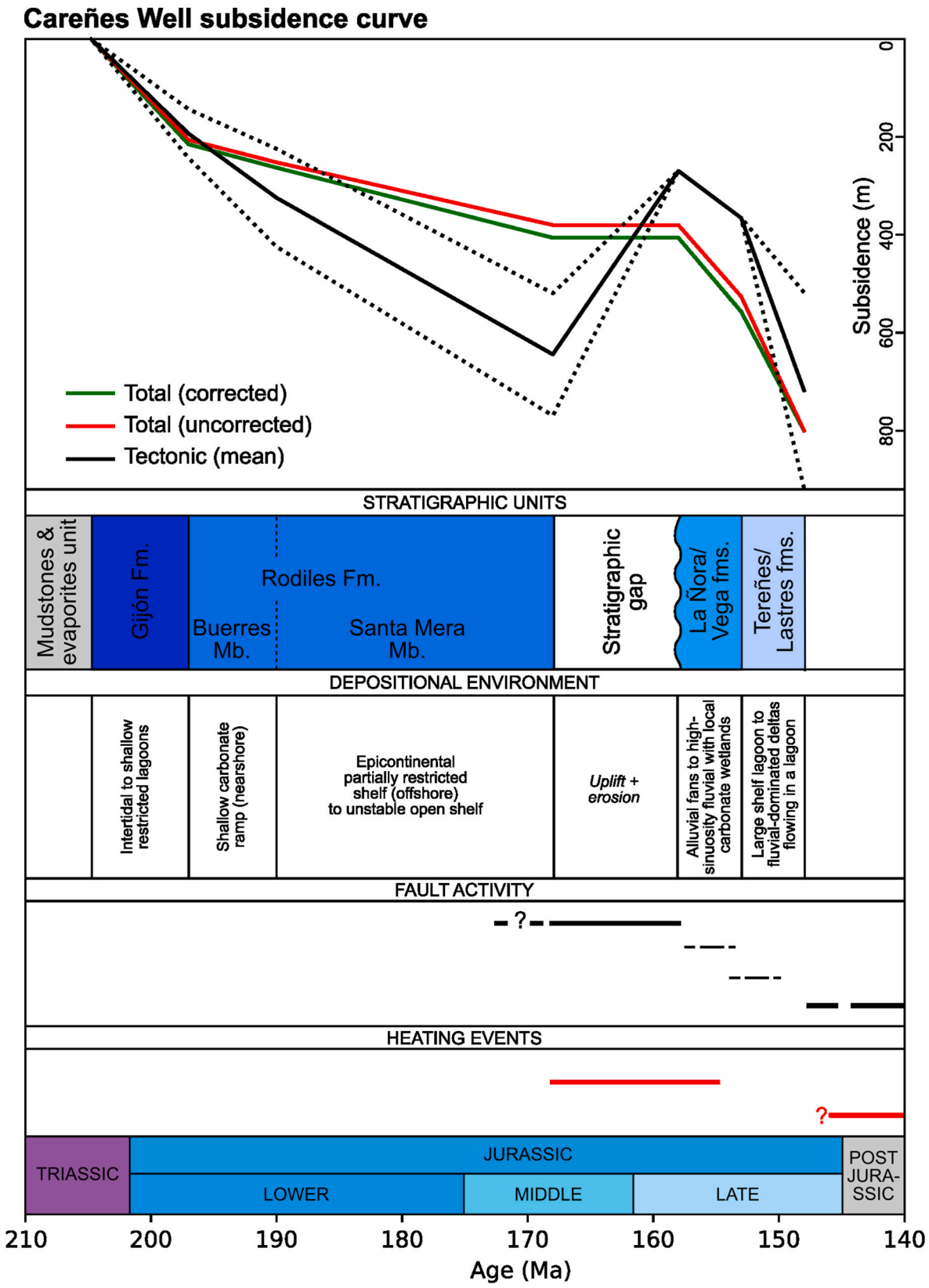

Fig. 8. Subsidence curves from the Late Triassic to the Late Jurassic. The stratigraphic units, their sedimentary environment, and the tectonic and thermal episodes are also indicated. The Careñes well was used to construct the curves as it has the most complete log for the Upper Triassic-Jurassic succession.

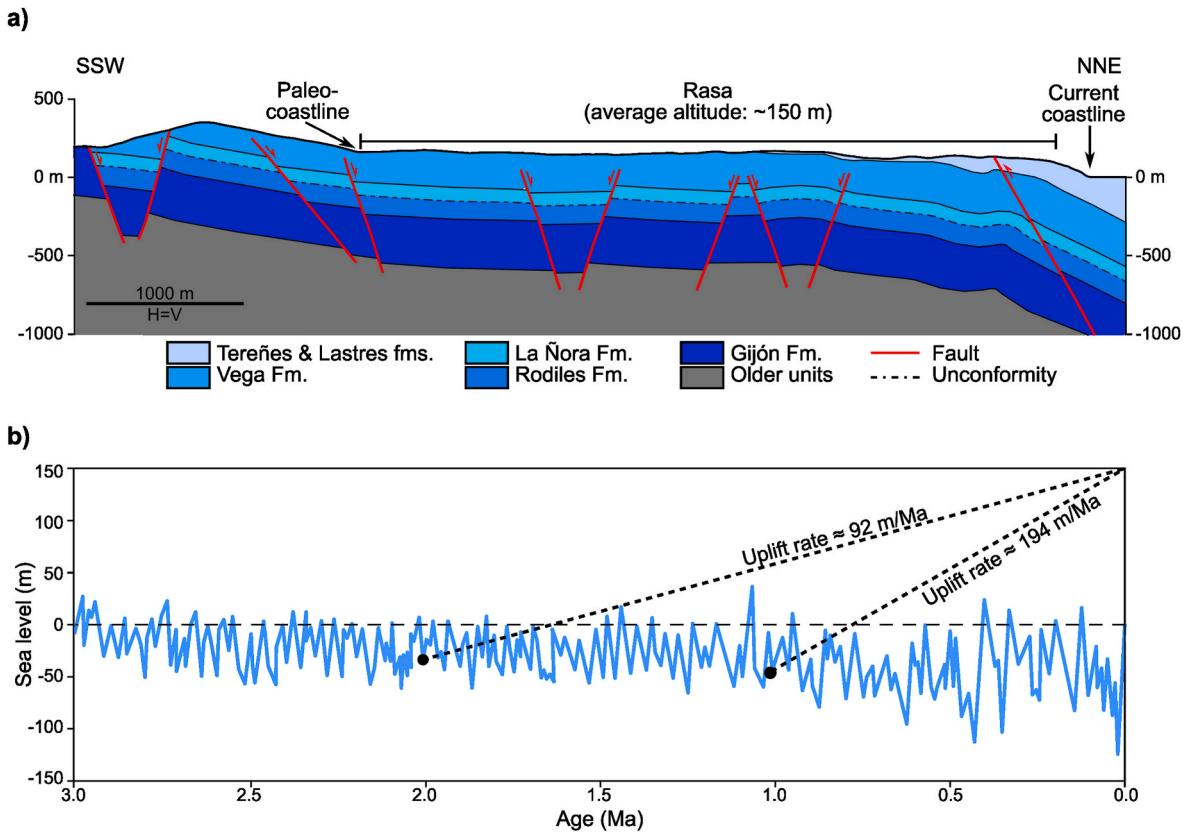

Fig. 9. a) Geological cross-section across the central part of the Asturian Basin showing the rasa developed on top of Mesozoic rocks. See Fig. 3 for location of the cross section. b) Sea level versus age graph showing two possible trajectories of the rasa assuming a present-day average altitude of 150 m above sea level, constant uplift rates and that the rasa was submerged at 1 and 2 Ma. The sea level curve has been taken from Miller et al. (2020).

This event reflects a higher heat flow than the younger one.

The vitrinite reflectance is related to temperature in such a way that the higher the reflectance the higher the temperature (e.g., Barker and Pawlewicz, 1994). The temperature values obtained from the samples collected in the lower carbonate succession are unrelated to depth; thus, the highest temperature values are not located in the deepest portions of the stratigraphic succession (Fig. 11a). In the study area the highest vitrinite reflectance values are approximately located around faults active before the intra-Jurassic unconformity (Fig. 12a and 13a) and they tend to decrease abruptly when moving away from these faults. Therefore, rather than burial, we believe the heat responsible for these vitrinite reflectance values could result from hydrothermal phenomena, so that faults might have facilitated the uprise of hydrothermal fluids, warming up the region around the faults and increasing the organic matter maturity. This hypothesis is consistent with the fluorite mineralizations in the mining districts of Villabona, Berbes and La Collada (see Fig. 3 for location) attributed to the mixing of metalliferous brines with surficial marine fluids through faults in Jurassic times (Sánchez et al., 2006, 2009, 2010). Moreover, around 25 km to the east-southeast of the Asturian Basin (Picos de Europa Region in the Cantabrian Zone), high-temperature cements related to the activity of dip-slip normal faults striking WNW-ESE to NW-SE of Late Jurassic to Early Cretaceous age have been documented (Flórez Rodríguez, 2024), which support the hydrothermal origin of the heat along faults.

El Puntal, Villaviciosa-La Conejera, Lastres, El Sable and Ribadesella faults show evidence of heating (Fig. 12a). Nonetheless, the high vitrinite reflectance value of 1.27 located near the Ribadesella Fault to the east of the study area (Fig. 13a) may be related to the younger event, given that the values for both the lower carbonate sequence and the upper detrital one are relatively similar. In addition to the faults depicted on the correlation panel in Fig. 12b, other faults could have also acted as conduits for the rise of hydrothermal fluids. For instance, the vitrinite reflectance values of 0.70–0.80 around La Collada area to the southwest of the study area (Fig. 13a) could be attributed to a set of NW-SE faults developed in this region (Figs. 3 and 6a) that were active before the unconformity. The vitrinite reflectance value of 1.15 to the southeast of the study area (Fig. 13a) could be related to the Llanera Fault, an E-W Mesozoic normal fault (Figs. 3 and 6a) inverted during the Alpine contractional event (Alonso et al., 2016).

Using the Barker and Pawlewicz (1994) equations to calculate temperatures from vitrinite reflectance and assuming that the heating was caused by hydrothermal sources, south of Lastres a maximum temperature of approximately 200 °C would have been reached, towards Ribadesella the highest value was 180 °C, similar to the one close to the Llanera Fault (170 °C), whereas along La Collada region the values were lower, about 120 °C (Fig. 13a and 14). There is a general temperature increase from west to east (from 35 °C to about 200 °C), a trend also seen in the fluorite deposits whose maximum temperatures pass from 90 °C (Villabona) to 130–140 °C (La Collada and Berbes, respectively) (Sánchez et al., 2009). Flórez Rodríguez (2024) calculated a temperature range of 75–400 °C (typically, 160–400 °C) for high-temperature calcite cements in the Picos de Europa Region.

The isocontours of the vitrinite reflectance, probably related to the extensional activity of the Ribadesella, El Sable, Lastres, Villaviciosa-La Conejera and El Puntal faults, seem to be truncated by the intra-Jurassic unconformity (Fig. 12a). Thus, the climax of this event would have taken place after the Rodiles Fm. deposition, but before the intra-Jurassic unconformity, i.e., between the Bajocian (middle part of the Middle Jurassic) and the Kimmeridgian (middle part of the Late Jurassic). The age of this heating event could be the same one than the heat flow responsible for the fluorite mineralization in areas close to the study area, dated as 185 ± 28 Ma ago (from the middle part of the Late Triassic

Table 2
Biostratigraphic data taken from Suárez-Vega (1974), Comas-Rengifo and Goy (2010), Comas-Rengifo et al. (2010, 2023), García-Ramos et al. (2010a, 2011), Goy et al. (2010) and Gómez et al. (2016a, 2016b) used to construct the subcrop map displayed in Fig. 7. See this figure for location of the logs. The thicknesses displayed in the table are accumulated mean values for the Jurassic carbonate succession up to each biozone. They have been calculated using logs throughout the whole basin in order to compare incomplete successions.

ID	LOCALITY	YOUNGEST BIOZONE	THICKNESS (M)
1	Peñarrubia to Gijón	*Jamesoni*	375
2	Serín	*Jamesoni*	375
3	Peón	*Ibex*	381
4	Careñes	*Murchisonae?*	448
5	El Puntal	*Opalinum*	445
6	W Rodiles	*Insigne*	434
7	E Rodiles	*Spinatum*	407
8	Santa Mera	*Sauzei*	469
9	Lastres Beach	*Variabilis*	425
10	La Griega Beach	*Sowerbyi*	459
11	Vega Beach	*Spinatum*	407
12	Ribadesella	*Bifrons*	420
13	Cimero	*Obtusum*	324
14	La Rimada to Pozo Los Lobos	*Jamesoni*	375
15	Argañosu	*Oxynotum*	334
16	Argañosu II	*Jamesoni*	375
17	La Vega Sariego	*Jamesoni*	375
18	Arbazal to Pandenes	*Raricostatum?*	354
19	Borines	*Thourasense?*	429
20	Caldones E	*Oxynotum?*	334
21	Deva	*Oxynotum?*	334
22	Deva to La Olla	*Ibex*	381
23	Arroes	*Raricostatum*	354
24	Casa del Marqués	*Jamesoni*	375
25	Seloriu to Santa Mera	*Serpentinus*	416
26	Castiello	*Margaritatus*	401
27	Venta del Pobre	*Bifrons*	420
28	Colunga	*Variabilis*	425
29	Lliberdón W	*Bifrons*	420
30	Lliberdón E	*Humphriesianum*	475

to the lower part of the Late Jurassic) using Sr and Nd radiogenic isotopes (Sánchez et al., 2006, 2010).

6.2. Heating event developed after the intra-Jurassic unconformity

The vitrinite reflectance values recorded in the upper detrital sequence for this event range between 0.33 and 1.24 (Table 3). As in the lower succession, the contours on a map increase from west to east (Fig. 10b). This event is associated with a lower heat flow than the older one.

Similarly to the lower carbonate succession, the vitrinite reflectance values obtained from the upper detrital succession, once converted onto temperatures and plotted on a graph versus depth, show that there is no relationship between temperatures and depth (Fig. 11b). This rules out the hypothesis that this heating event was caused by burial. The highest vitrinite reflectance values are located near faults active after the intra-Jurassic unconformity (with both normal and reverse displacements) and when moving away from these faults, the vitrinite reflectance values decrease abruptly (Fig. 12b and 13b). These observations suggest that the faults were the conduits through which the hot hydrothermal fluids would have circulated and would have been responsible for the organic matter maturation. However, the conclusions regarding this young event must be taken carefully, given the scarcity of the data.

The maximum vitrinite reflectance value was attained near the Ribadesella Fault (Figs. 12b and 13b). As mentioned above, this maximum (1.24) is very similar to that recorded in the stratigraphic succession below the unconformity (1.27). Other faults could have also acted as conduits for the rise of hydrothermal fluids. Thus, the maximum above 0.60 near a locality called Oles in the north part of the Asturian Basin (Fig. 13b) could be attributed to a fault active after the intra-Jurassic unconformity (Figs. 3, 6b and 6c).

Using the Barker and Pawlewicz (1994) equations to convert vitrinite reflectance values to temperature assuming hydrothermal heating, a maximum temperature of around 180 °C would have been reached near Ribadesella, whereas the values in the Oles region were lower, about 110 °C (Fig. 13b and 14).

The occurrence of oncoids within the Vega Fm. aligned along a fault (García-Ramos et al., 2010c; Uzkeda, 2013; Uzkeda et al., 2016) indicates the presence of hot fluids circulating along a fault coetaneous to this stratigraphic unit. This fluid migration could have contributed to the maturity of the organic matter of the lower part of the detrital succession, however, it does not explain why the upper part of the detrital succession (Tereñes and Lastres fms.) also recorded a thermal event (Fig. 12b). Another aspect that may contribute to unravel the age of this heating event is the Lastres Fm. samples collected in the Oles region. A vitrinite reflectance value of 0.72, using phlobafinite as a marker, was measured by Suárez-Ruiz et al. (2006) in the Oles region. These authors highlight the discrepancies between the values obtained using two components of the vitrinite: phlobafinite (0.72) and ulminite (0.39). They attribute it to the perhydrous character of the sample, which would have been the result of impregnation by oils during an early diagenetic stage (Suárez-Ruiz et al., 1994; Jiménez et al., 1998). The fact that there was oil generation immediately after the deposition of the Upper Jurassic Lastres Fm. suggests that this heating event might have been responsible for its generation and, therefore, its age would be close to Late Jurassic. It is not very likely that this heating event is related to the Cenozoic Alpine contraction. Thus, in the Picos de Europa region, Flórez Rodríguez (2024) described low-temperature calcite cements (15–85 °C) that precipitated along strike slip-reverse faults attributed to the Cenozoic Alpine contraction. Such temperature values would not be enough to explain the organic matter maturity reached in regions such as Oles and Ribadesella, that would have required temperatures over 100 °C.

7. Tectono-thermal evolution of the Asturian basin from Late Triassic to present-day

After a moderate and approximately constant tectonic subsidence rate of approximately 20 m/Ma (Fig. 8), during which an Upper Triassic-Middle Jurassic marine succession was deposited (Fig. 2), a tectono-thermal event took place (Fig. 15). The age of this extensional event, recorded by a stratigraphic gap between the youngest part of the Late Triassic-Middle Jurassic succession and the intra-Jurassic unconformity (Fig. 2), ranges from post-Bajocian times (middle part of the Middle Jurassic) to pre-Kimmeridgian times (lower part of the Late Jurassic). During this event, at least, the El Puntal, Villaviciosa-La Conejera, Lastres, El Sable and Ribadesella faults were active. This event involved rapid tectonic uplift at a rate of 40 m/Ma (Fig. 8), specially pronounced in the western part of the basin (Figs. 3 and 4a), which caused basin emersion. In addition, a large gentle syncline, whose trough is approximately located in the central-eastern part of the basin, developed in the coastal part of the basin (Fig. 4a). This process was accompanied by normal faulting (Fig. 4a, 6a and 7), consisting of formation of new faults and possible reactivation of inherited structures. Most of the faults active during this event strike NW-SE (Figs. 6 and 7) and their maximum throw reached tens of meters (Table 1). The rise of hydrothermal fluids through several faults (Fig. 12a and 13a) caused heating that increased from west to east, reaching maximum temperatures of 200 °C (Fig. 14) and leading to organic matter maturation.

Significant erosion occurred, causing an intra-Jurassic unconformity that truncated the Palaeozoic, Triassic and Lower-Middle Jurassic layers, as well as the structures developed during the pre-unconformity extensional event (Figs. 2, 3, 4a and 15). Moderate tectonic subsidence on the order of 25 m/Ma facilitated the resumption of sedimentation in a continental environment above the unconformity during the Late Jurassic (Fig. 8). However, soon the subsidence reached high values of

Table 3
Vitrinite reflectance values taken from Suárez-Ruiz (1988), Suárez-Ruiz and González Prado (1995) and Suárez-Ruiz et al. (2006). Blue rows: samples from the Upper Triassic-Jurassic carbonate sequence. Orange rows: samples from the Jurassic detrital succession. Temperatures estimated using the Barker and Pawlewicz (1994) equation for hydrothermal processes. See Fig. 10 for location of the samples.

ID	LOCALITY	UNIT	VALUE	TEMP. (°C)
1	Avilés E	Gijón Fm.	<0.50	<64
2	Overo	Gijón Fm.	<0.50	<64
3	Peñarrubia Beach	Rodiles Fm.	0.39	32
4	Serín Beach	Rodiles Fm.	0.40	35
5	Porceyo	Gjión Fm.	0.50	64
6	Estaño	La Ñora – Lastres fms.	0.38	28
7	La Ñora W	La Ñora Fm.	0.38	28
8	La Ñora E	Lastres Fm.	0.38	28
9	España W	Lastres Fm.	0.46	53
10	España E	Lastres Fm.	0.33	10
11	Arroes	Rodiles Fm.	0.75	115
12	Agüera	Gijón Fm.	<0.50	<64
13	Argañoso	Gijón Fm.	0.50	64
14	La Rimada 1	Gijón Fm.	0.70	107
15	La Rimada 2	Gijón Fm.	0.80	124
16	Altu La Fumarea 1	Rodiles Fm.	0.70	107
17	Altu La Fumarea 2	Rodiles Fm.	0.80	124
18	El Puntal	Rodiles Fm.	0.88	136
19	Rodiles Beach	Gijón Fm.	0.84	130
20	La Conejera Inlet	Rodiles Fm.	0.85	131
21	Lastres Harbour	Lastres Fm.	0.48	58
22	Lastres Beach 1	Rodiles Fm.	0.83	128
23	Lastres Beach 2	Vega Fm.	0.52	69
24	La Griega 1	Tereñes Fm.	0.50	64
25	La Griega 2	Rodiles Fm.	0.75	115
26	Huerres Beach	Rodiles Fm.	0.93	143
27	Colunga-Lastres	Rodiles Fm.	1.40	195
28	Colunga	Rodiles Fm.	1.53	207
29	Vallobal	Rodiles Fm.	1.15	170
30	Vega Beach	Gijón Fm.	1.18	173
31	Ribadesella Beach	Rodiles Fm.	1.27	183
32	Tereñes	Tereñes – Lastres fms.	1.02	155
33	Las Atalayas	Lastres Fm.	1.24	180
34	Oles mine	Lastres Fm.	0.72	110

approximately 70 m/Ma, and sedimentation shifted to be dominated by lagoonal environments. This tectonic subsidence, occurring after the intra-Jurassic unconformity and during the sedimentation of the middle Upper Jurassic sequence, could be interpreted as thermal subsidence due to lithosphere cooling after the pre-unconformity extensional event, during which high temperatures were reached. During this thermal subsidence event, occasional small-scale syn-sedimentary normal faults still developed, and locally hot fluids circulated along them (Fig. 14).

Between Late Jurassic and pre-Barremian Early Cretaceous time, another tectono-thermal event occurred (Fig. 15). This extensional event caused the reactivation of many normal faults active during the older extensional event and the modification of part of the geometry of the large gentle syncline previously formed in the coastal part of the basin (Fig. 4b). The throws of the faults increased up to hundreds of meters (Table 1), most of them with NW-SE strikes (Fig. 6b). A few faults allowed circulation of hot fluids along them (Fig. 12b and 13b), albeit the heat was weaker than that in the older thermal event, since maximum temperatures reached 180 °C in the eastern portion of the basin (Fig. 14).

At first glance, the Middle-Late Jurassic and the Late Jurassic-Early Cretaceous events, both involving extensional faulting and heat, might be considered as a single tectono-thermal event. However, the presence

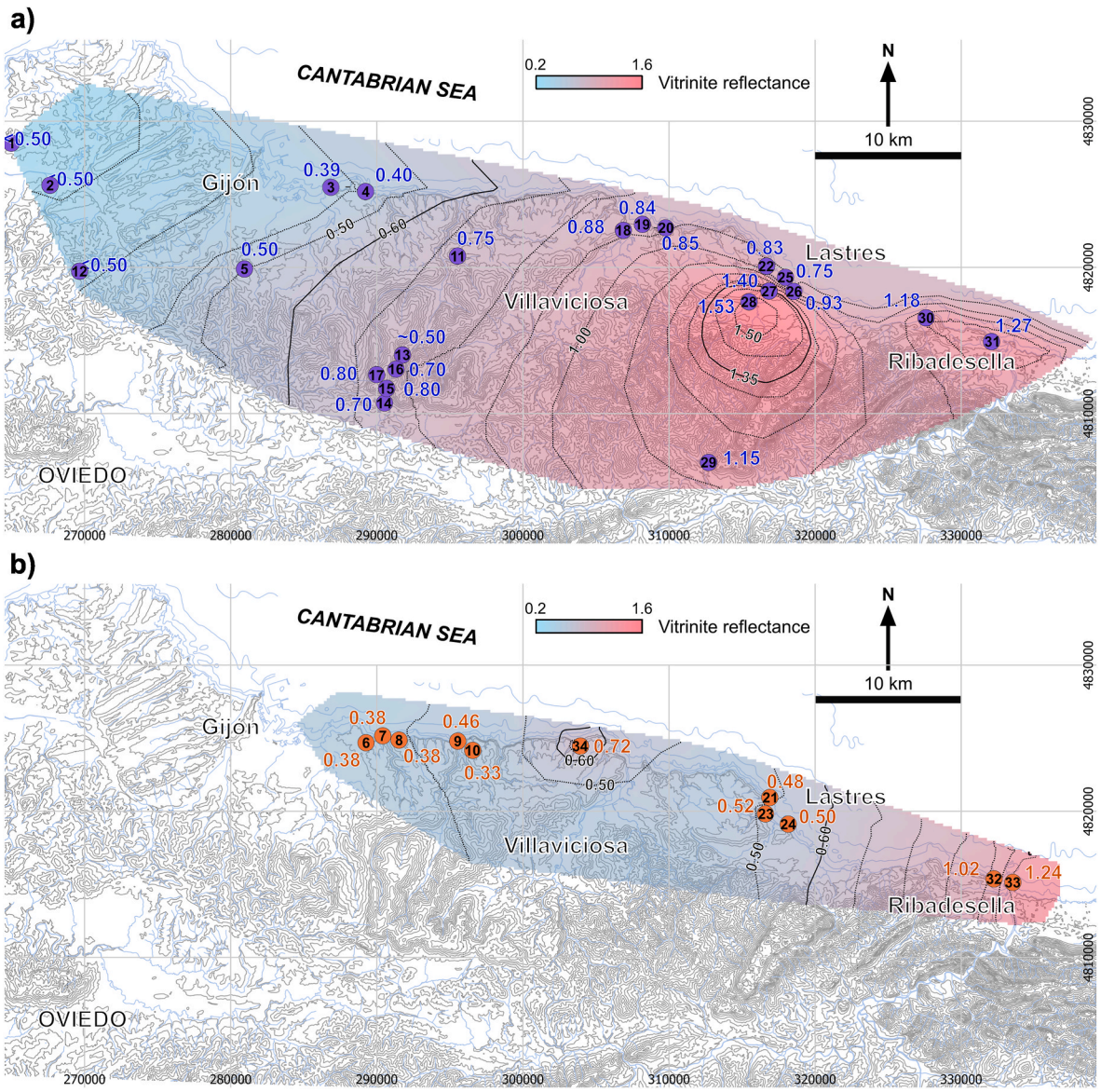

Fig. 10. Maps constructed contouring the vitrinite reflectance values for: a) the Upper Triassic-Jurassic carbonate rocks and b) the Jurassic detrital rocks. Interval between vitrinite reflectance contours (dotted lines): 0.10. The vitrinite reflectance curves of 0.60 (beginning of the oil formation window) and 1.35 (beginning of the window of wet gas formation) are shown with a solid line. The data used are listed in Table 3.

of the intra-Jurassic unconformity between both and the lack of significant syn-sedimentary tectonic structures during the deposition of the middle Upper Jurassic sequences suggests that there was a tectonic quiescence period between both (Figs. 8 and 15). Thus, these observations support two distinct tectono-thermal events.

During part of the Paleogene and Neogene, a contractional event produced the development of reverse faults with dominant E-W strike, whose throws reach several tens of meters, and inversion of previous normal faults, decreasing their normal displacement by tens of meters (Fig. 4c and 6c, and Table 1). However, reverse slip might not have been the only type of reactivation, as there are examples of faults along the basin that suffered buttressing, and/or strike-slip reactivation (such as the NE-SW Villaviciosa-La Conejera Fault). In the coastal part of the basin, a pop-up type structure was generated between two faults to the west and the large syncline became two smaller close synclines separated by a horst-cored anticline (Fig. 4c).

During the Quaternary, at least the coastal part of the Asturian Basin, which corresponded to a marine abrasion platform (Fig. 9a), emerged at a very rapid rate of approximately 92–194 m/Ma (Fig. 9b). This phenomenon was accompanied by development of earthquakes associated with one of the currently active faults (e.g., López-Fernández et al., 2018; Fernández-Viejo et al., 2021).

8. Implications for hydrocarbon exploration

The subsurface of the offshore portion of the Asturian Basin has proved to produce oil and gas and to have reservoir rocks with adequate porosity and permeability values to store hydrocarbons (e.g., Riaza Molina, 1996; Gutiérrez Claverol and Gallastegui, 2002; Gutiérrez Claverol et al., 2002, 2005; Saénz de Santamaría and Gutiérrez Claverol, 2013). However, these authors point out that the variation of productive parameters at short distances and the low reservoir/cover ratio do not favour the existence of economically viable findings, and furthermore, the complex geological structure resulting from basin inversion makes it difficult to find fields of suitable size.

For kerogen type II, such as that identified within the Upper Triassic-Jurassic carbonate succession (Suárez-Ruiz, 1988; Suárez-Ruiz and González Prado, 1995), the early oil generation typically commences

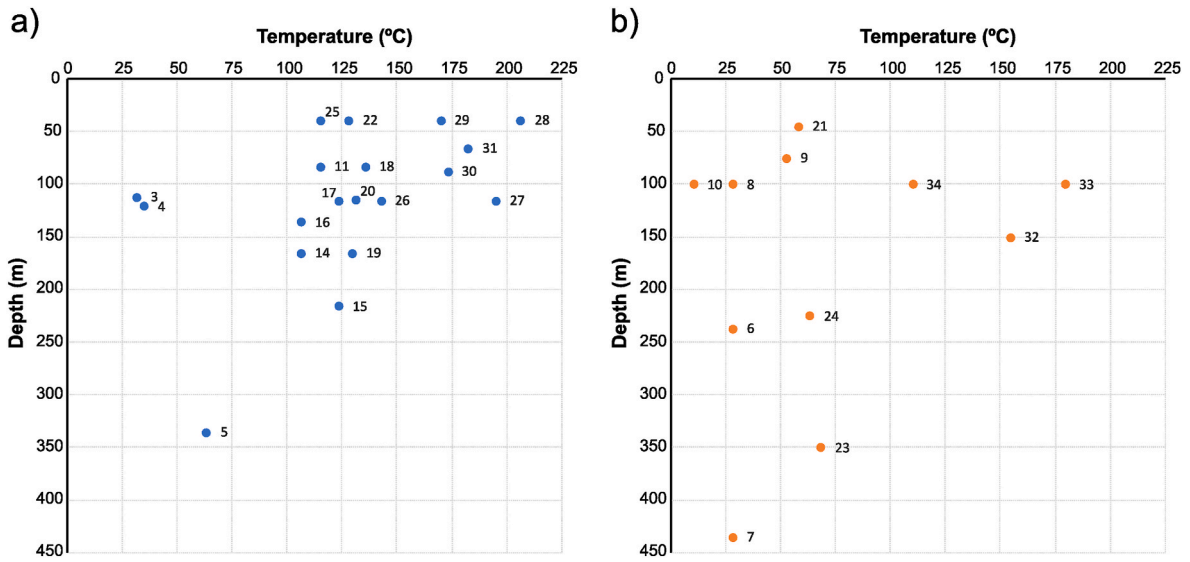

Fig. 11. Depth versus temperature plots for: a) the old heating event developed before the intra-Jurassic unconformity (depth: meters below the Rodiles Fm. top, taking the most complete stratigraphic log as reference) and b) the young heating event developed after the intra-Jurassic unconformity (depth: meters below the Lastres Fm. top, taking the most complete stratigraphic log as reference). The labels next to each point correspond to the ID of the samples shown in Table 3.

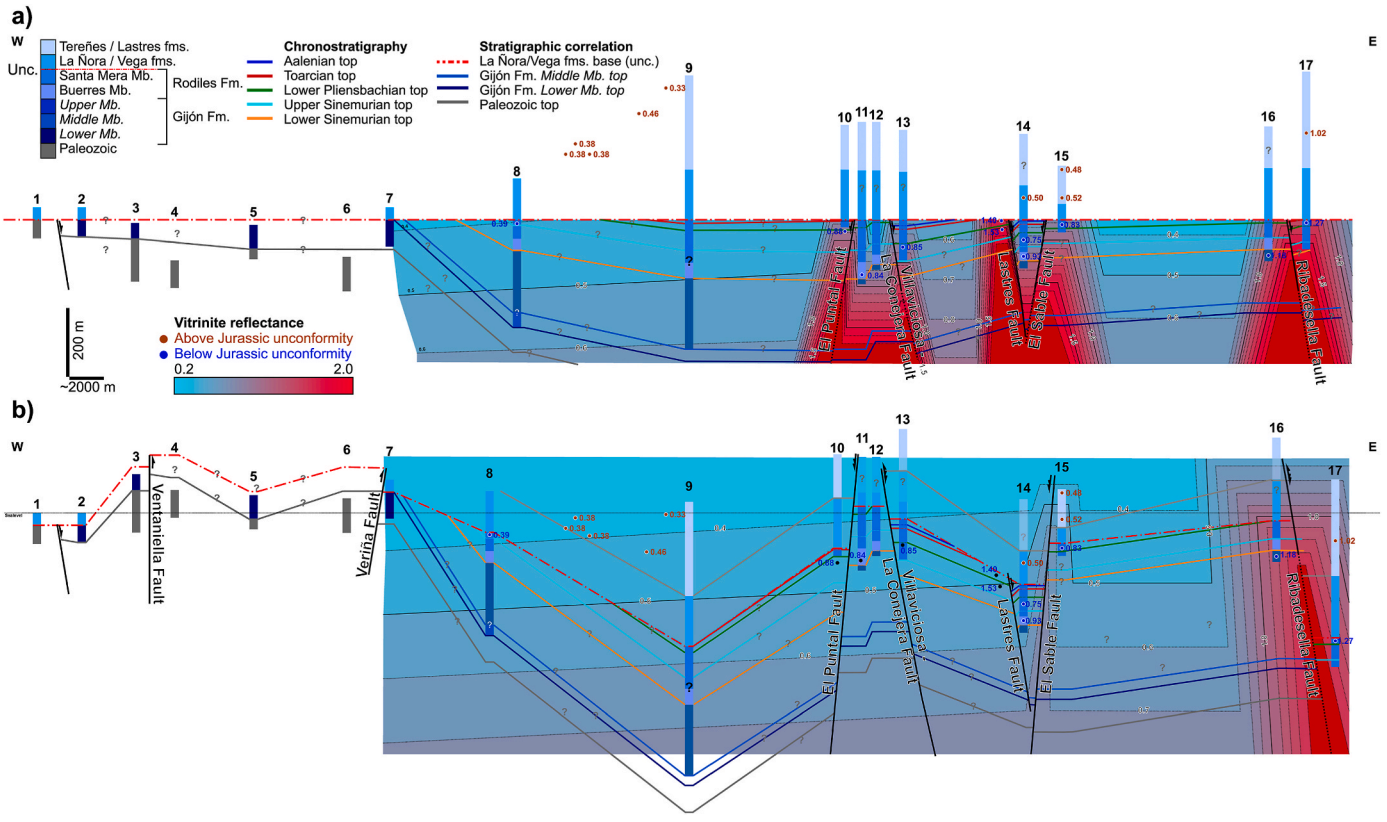

Fig. 12. Stratigraphic correlation panels shown in Fig. 4a and c including vitrinite reflectance values from Table 3, as well as vitrinite reflectance isocontours, for: a) the old heating event developed before the intra-Jurassic unconformity and b) the young heating event developed after the intra-Jurassic unconformity. See location of stratigraphic logs in Fig. 3.

when vitrinite reflectance values reach a value of 0.60, whereas the wet gas window starts at 1.35 (Dow, 1977; Senftle and Landis, 1991; Dembicki, 2009, 2022). Given this, the isocontour vitrinite reflectance maps constructed using interpolation algorithms without considering a possible structural control (Fig. 10) show a relatively wide area of around 750 km^2 that reached the oil window generation and a smaller one, about 40 km^2, where conditions for gas generation were met. However, when the vitrinite reflectance maps are created taking into account the possible control exerted by the faults over the organic matter maturity (Fig. 13), the regions susceptible of having reached the oil and gas windows are much more reduced (146 and 10 km^2, respectively) and, consequently, there would have been less hydrocarbon

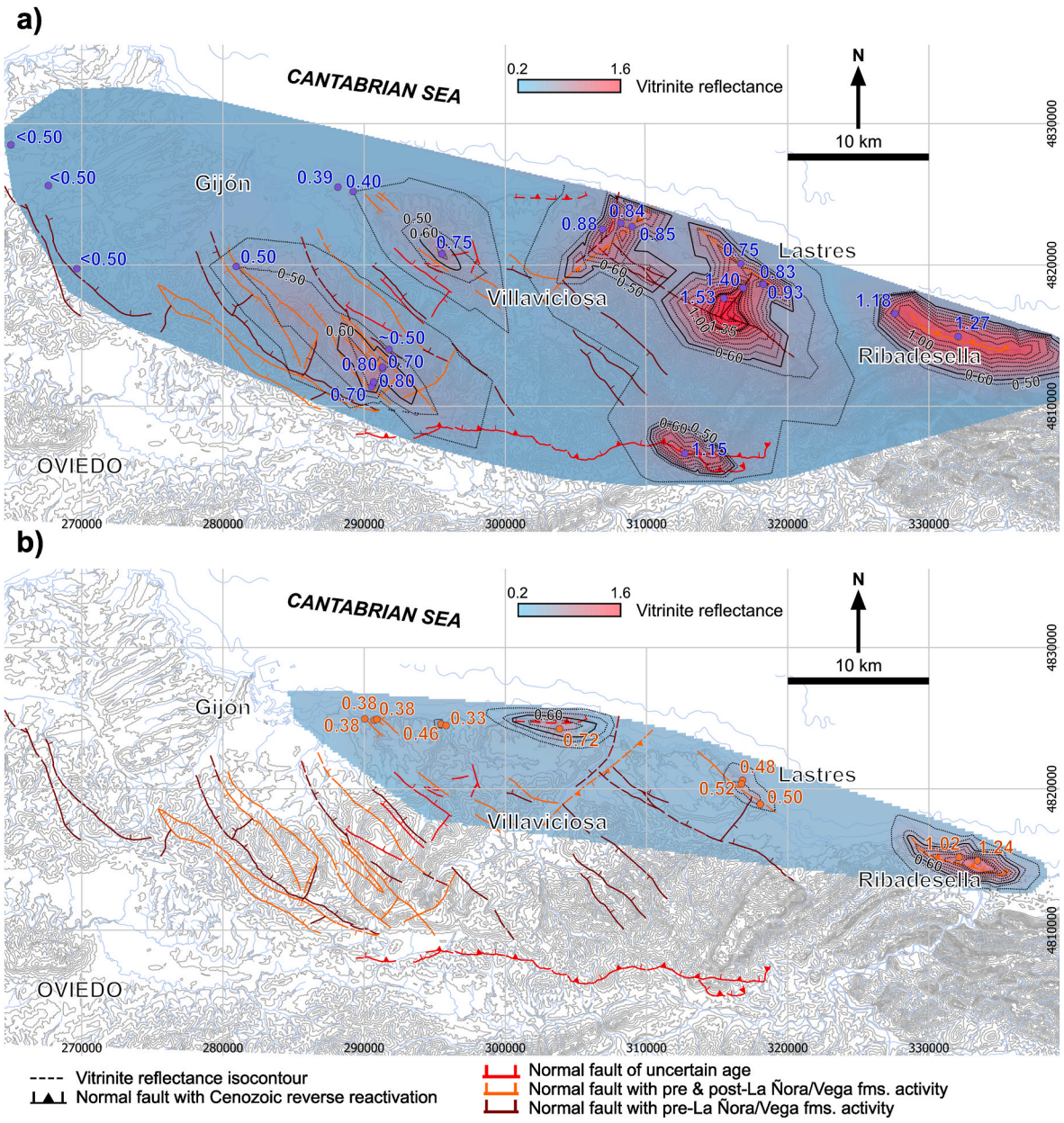

Fig. 13. Vitrinite reflectance maps constructed taking into account the correlation panels shown in Fig. 12: a) values for the Upper Triassic-Jurassic carbonate rocks and b) values for the Jurassic detrital rocks. Interval between vitrinite reflectance contours (dotted lines): 0.10. The vitrinite reflectance curves of 0.60 (beginning of the oil formation window) and 1.35 (beginning of the window of wet gas formation) are shown with a solid line. The data used are listed in Table 3.

generation than expected. Regarding the younger heating event, the map considering the structural control shows that the conditions for gas generation were not reached, and the oil conditions were reached in an area of less than 20 km^2. Thus, another factor to explain the lack of economically viable hydrocarbon fields in this region is the fact that large enough volumes of hydrocarbons were not generated because of the reduced hydrocarbon kitchen.

Another element that would have acted against the formation of large reservoirs is the timing of the old heating event, which seems to have been the most important one. When it occurred, i.e., Bajocian-Kimmeridgian, there were neither potential reservoir rocks above the unconformity, nor seals above the reservoir, and this would have impeded the formation of traps and allowed the loss of the migrating hydrocarbons.

9. Implications for the geodynamic models of the north Iberian margin

Various geodynamic models have been proposed to account for the Mesozoic evolution of the North Iberian margin and the opening of the Bay of Biscay: i) anticlockwise rotation of Iberia (e.g., Srivastava et al., 2000; Sibuet et al., 2004; Vissers and Meijer, 2012); ii) left-lateral strike slip (e.g., Le Pichon and Sibuet, 1971; Olivet, 1996; Stampfli et al., 2002; Handy et al., 2010); iii) transtension (King et al., 2021); iv) transtension followed by minor orthogonal extension (Jammes et al., 2009); v) successive stages of transtension in a diffuse plate boundary (Asti et al., 2022). Because of the limited extension of our study area compared to that of the North Iberian margin, and the absence of most of the Cretaceous syn-rift sequence in the region, it does not seem reasonable to support one or several models above the others. Despite this, the work presented here may help to understand the possible evolution of this

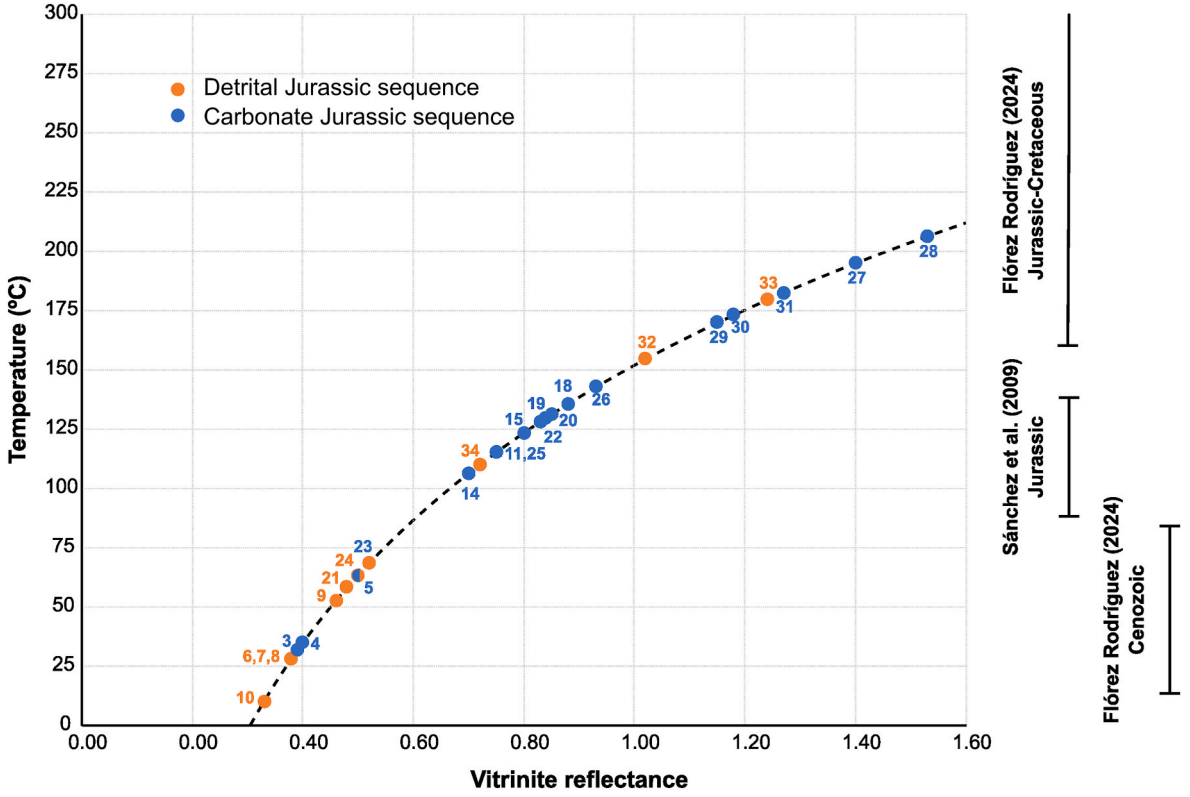

Fig. 14. Temperature versus vitrinite reflectance graph showing the values measured in the Asturian Basin. The right part of the figure includes the range of temperatures obtained for cements along faults (Flórez Rodríguez, 2024) and fluorite mineralization (Sánchez et al., 2009). The temperatures have been calculated using the Barker and Pawlewicz (1994) equation for hydrothermal processes. The labels next to each point correspond to the ID of the samples shown in Table 3.

portion of the North Iberian margin regarding two main aspects: i) the amount of extension and ii) the role of the Ventaniella Fault.

9.1. *Amount of extension*

The onshore portion of the Asturian Basin has been typically considered as part of the necking domain of the Mesozoic rift that took place in the Bay of Biscay (e.g., Tugend et al., 2015a; Cadenas et al., 2018, 2020; King et al., 2023). Given that the necking domain is partially within the high-β extensional systems (Tugend et al., 2015b), a relatively high amount of extension, accommodated by gently dipping faults and notable fault slips, should be expected. However, in the study area normal faults usually dip above 50°, and display throws of less than 300 m and heaves of no more than 80 m (Fig. 4a and b). Considering both the high fault dip and the small fault motion, it seems more plausible that the emerged portion of the Asturian Basin, rather than part of the necking domain of the hyper-extended Biscay Rift System, would correspond to a proximal region, with less amount of extension and a structural architecture similar to that of the classical rift systems formed by grabens and half-grabens. Our observations fit better in the multi-stage model proposed by Cadenas et al. (2020) within the "Diffuse Gijón-Ribadesella Rift System" (formed by horst and half-grabens). The structural style seen onshore is comparable to that of the Gijón-Ribadesella system, albeit with two main differences. The first one is that, unlike the offshore portion of the basin (Cadenas et al., 2020), onshore there are evidence of normal fault activity after the Triassic rift at least twice: before and after the intra-Jurassic unconformity (Figs. 4, 6 and 7). The second difference is that the large normal faults onshore cut and offset most of the Mesozoic succession from the Triassic to the Cretaceous, while offshore there are normal faults that involve the pre-evaporitic Triassic succession and the underlying rocks, and others that affect only the post-evaporitic succession (Cadenas et al., 2020). The last difference may be due to the extremely different thickness of the Triassic evaporites offshore and onshore. Thick evaporitic sequences, including salts, have been drilled offshore (more than 600 m in the MC-K1 well according to Cadenas and Fernández-Viejo, 2017, about 500 m in the MC-B4 as stated by Zamora et al., 2017, see wells location in Fig. 16) and salt-related structures have been extensively interpreted (e.g., Boillot et al., 1979; Cadenas and Fernández-Viejo, 2017; Zamora et al., 2017; Cadenas et al., 2020). In contrast, the evaporite sedimentation was less significant onshore, with successions of 40–60 m thickness in the Vilorteo and Cantavieyo wells (see wells location in Fig. 3) located in La Collada mining district (Pieren et al., 1995; Barrón et al., 2006), and salt-related structures have not been documented, except for sporadic breccias within the Gijón Fm. interpreted as dissolution of underlying evaporites and subsequent collapse (Barrón et al., 2002, 2006; González-Fernández et al., 2004a). The presence of thick evaporite sequences offshore may have facilitated the creation of salt rollers and hindered normal fault propagation from deeper to shallower parts of the stratigraphic succession, which has not occurred onshore where evaporites are thinner.

9.2. *Role of the Ventaniella Fault*

In large-scale and offshore studies, the Ventaniella Fault (Figs. 1, 3 and 16) has traditionally been considered as a main tectonic boundary or an active fault controlling the Mesozoic rifting events (e.g., De Vicente et al., 2011; Roca et al., 2011; Fernández-Viejo et al., 2014; Tugend et al., 2015a; Cadenas et al., 2018, 2020; López-Gómez et al., 2019; Asti et al., 2022). However, some observations in the Asturian Basin are not fully aligned with such interpretation. Below, we will examine the role played by the Ventaniella Fault during the different Mesozoic events including a brief comment about the Triassic rift previous to the events this paper is focused on.

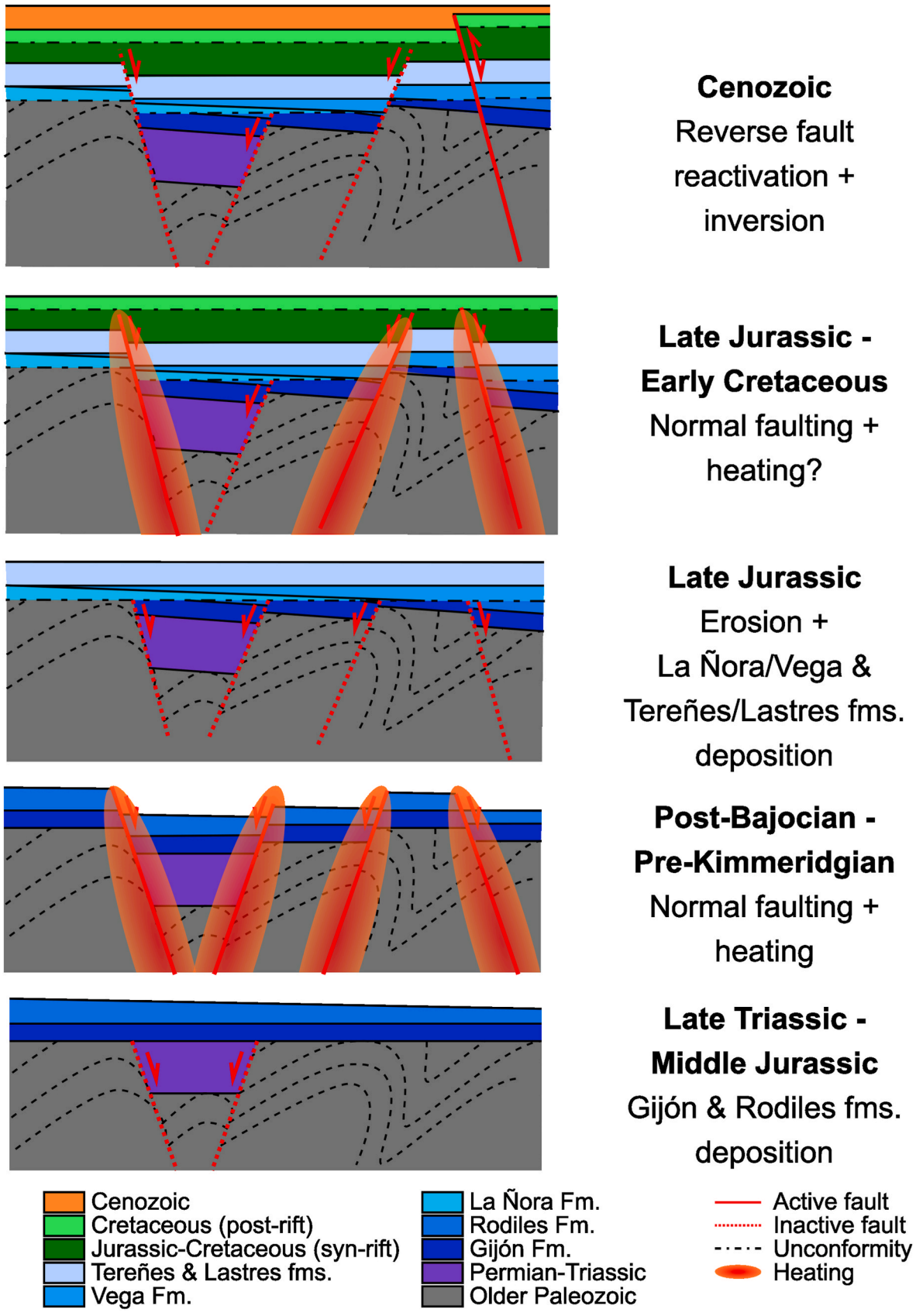

Fig. 15. Conceptual sketch showing the most significant events undergone in the onshore portion of the Asturian Basin since Late Triassic-Early Jurassic times.

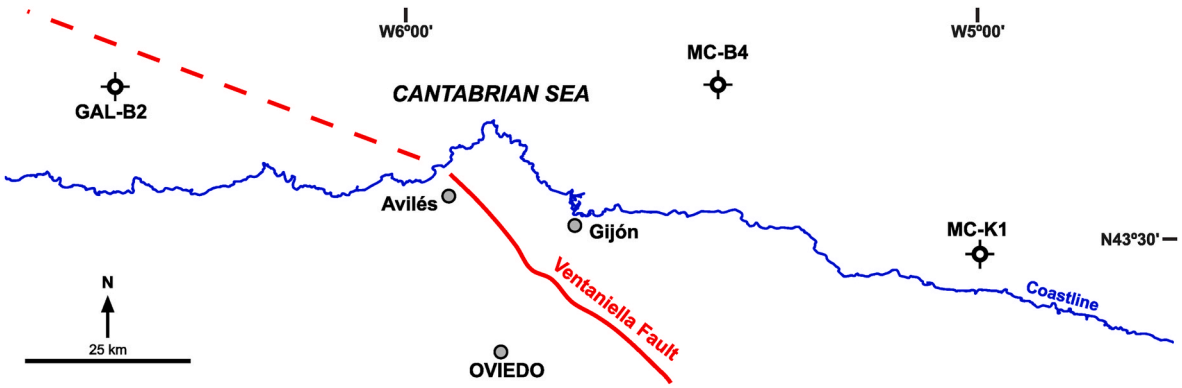

Fig. 16. Map showing the location of the Ventaniella Fault and the offshore wells GAL-B2, MC-B4 and MC-K1.

According to López-Gómez et al. (2019) the Ventaniella Fault is the southwest boundary of the Gijón-Villaviciosa Triassic sub-basin. Despite this, these authors acknowledge that Triassic deposits were found in the offshore GAL-B2 well (see well location in Fig. 16) located in the southwest block of the Ventaniella Fault. In addition, onshore, the youngest Triassic syn-rift unit, called Fuentes Fm (Suárez-Rodríguez, 1988) or Transición Fm. (López-Gómez et al., 2019), has been mapped in the southwest block of the Ventaniella Fault, just south of La Pola Siero locality (Merino-Tomé et al., 2023) (south-central part of the geological map illustrated in Fig. 3). This stratigraphic unit crops out along a NE-SW trending syncline, whose axis plunges to the NE, bounded by reverse faults (probably inverted Permian normal faults), according to López-Gómez et al. (2019). The decrease in thickness of this stratigraphic unit from approximately 260 m to about 70 m towards the southwest is due to its truncation by the erosive base of the overlying post-rift Cretaceous Pola de Siero Fm. Thus, although the Ventaniella Fault may have exerted a certain control on the Triassic rifting event, its role as a main tectonic boundary during the Triassic is doubtful. In fact, the NE-SW trend of this unit might be attributed to the activity of faults parallel to the Villaviciosa-La Conejera Fault and its southwestern continuation, the La Peña Fault (Alonso et al., 2016) which would correspond to the negative inversion of Variscan structures such as the Pajares Fault/Backthrust (Aller, 1986; Alonso et al., 2009b).

The Late Triassic and Early Jurassic, i.e., during the sedimentation of the Gijón and Rodiles fms., were periods of tectonic quiescence during which the Ventaniella Fault would have been inactive. If the fault had been active, or acted as a basin boundary, sedimentary environment and thickness variations would be expected in the vicinity of the fault. However, according to Suárez-Vega (1974) the Rodiles Fm. features in the stratigraphic column closest to the Ventaniella Fault (column 17 in Fig. 7) are similar to those in the coastal stratigraphic columns far from the fault.

The Ventaniella Fault does not seem to have played an important role during the extensional event occurred just before the intra-Jurassic unconformity either. The correlation panel flattened to the unconformity (Fig. 4a) shows that, from El Puntal Fault to the west, La Ñora Fm. lies unconformably over older rocks. La Ñora Fm. rests upon the Rodiles Fm. in the central part of the Asturian Basin, eventually truncating it completely to the west of the column 8 in Figs. 3 and 4a. Further to the west, La Ñora Fm. overlies the Gijón Fm., completely truncating it to the west of the column 2 in Figs. 3 and 4a. From this point westward, La Ñora Fm. rests upon Palaeozoic rocks (Figs. 3 and 4a). This westward deepening of the erosion might be explained by a pre-unconformity regional tilting to the east. Had the Ventaniella Fault been active during this period of time, there should be an abrupt change of the erosional level between the stratigraphic columns located in its northeastern fault block and those located in its southwestern fault block. However, neither the geological and subcrop maps nor the stratigraphic correlation panels show evidence of this; rather, they indicate a progressive deepening of erosion (Figs. 3, 4a and 7).

Patches of Lower Cretaceous sediments lay unconformably over Palaeozoic rocks in the vicinity of the town of Antromero (Arbizu et al., 1995, 2015; González-Fernández et al., 2004b) (northwestern part of the map illustrated in Fig. 3) in the northeastern block of the Ventaniella Fault which, according to previous authors, is supposedly the sunken fault block during the Late Jurassic - pre-Barremian Early Cretaceous extensional event. The Lower Cretaceous stratigraphic units mapped are the Barremian Peñaferruz Fm. and the Barremian(?)-Aptian Antromero Fm., both belonging to the basal part of the post-rift sequence (Alonso et al., 2016), while the Palaeozoic stratigraphic units belong to the pre-rift sequence in relation to this extensional event. The fact that, in the supposedly sunken fault block, the post-rift sequence lays above the pre-rift sequence without any syn-rift sediments in between would indicate that the Ventaniella Fault was inactive or that it had very little displacement and the thin syn-rift sequence deposited was eroded before deposition of the post-rift sequence (Fig. 17a). The Asturian Basin faults that played an important role during the Late Jurassic - pre-Barremian Early Cretaceous extensional event, such as the Llanera Fault, exhibit post-rift sequences upon syn-rift sediments in the hangingwall, and post-rift sequences above pre-rift rocks in the footwall (Alonso et al., 2016). Currently, the Ventaniella Fault has a reverse throw of about 50 m (Table 1 and Fig. 4c). If the Ventaniella Fault indeed played an important role during the Late Jurassic - pre-Barremian Early Cretaceous extensional event, then the reverse throw it experienced during the Cenozoic Alpine contractional event must have been very significant in order to compensate all the normal throw and end up with 50 m reverse throw. A significant throw during the Cenozoic Alpine contraction could possibly have led to the development of a thick syn-inversion succession related to the fault (Fig. 17b). However, syn-inversion sediments of Cenozoic age related to the Ventaniella Fault have not been documented. The only syn-inversion sequences in the onshore portion of the Asturian Basin occur in the Oviedo Basin (Fig. 3), a basin fed by the erosion of the hangingwall of the E-W striking Llanera Fault (García-Ramos and Gutiérrez Claverol, 1995; Alonso et al., 1996). Both the absence of a syn-rift sequence between the post- and pre-rift sequences in the northeastern block of the Ventaniella Fault, as well as the absence of syn-inversion sediments associated with the fault (Fig. 17a), call into question the role attributed to the Ventaniella Fault as one of the main structural elements controlling the Late Jurassic - pre-Barremian Early Cretaceous rift in the onshore portion of the Asturian Basin.

10. Conclusions

From Late Triassic to present-day, the Asturian Basin experienced two extensional events and a contractional one. The oldest extensional episode consisted of uplift, normal faulting and gentle folding, as well as heating. It took place from the middle part of the Middle Jurassic to the

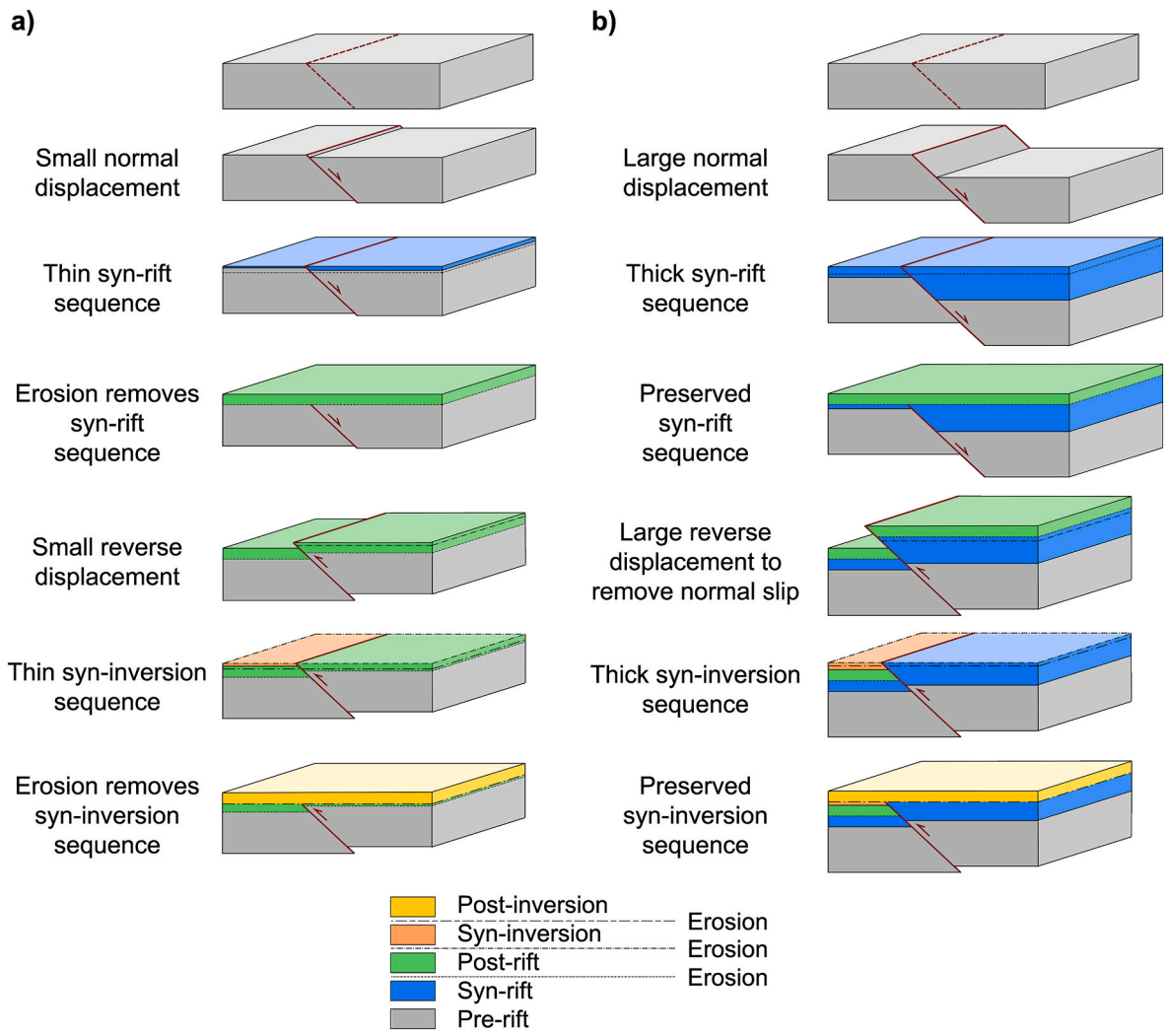

Fig. 17. Conceptual sketches of normal faults reactivated as reverse faults, highlighting the main disparities as a consequence of different amounts of fault motion during the extensional and contractional events. a) small normal and reverse fault displacements, and b) large normal and reverse fault displacements. The path a) is the one proposed here for the Ventaniella Fault.

middle part of the Late Jurassic. The youngest extensional event was responsible for reactivation of some faults and a slightly weaker heating. Its timing is less constrained, as it could have happened from Late Jurassic to Early Cretaceous time. These two events are separated by an intra-Jurassic unconformity, as well as by a thermal subsidence period. During the contractional event in Paleogene-Neogene time, reverse faults and some folds formed, and some older faults were reactivated, inverted and underwent buttressing effects. Neotectonics during Quaternary times led to basin emersion accompanied by some seismogenic active faults.

The integration of cartographic, structural, biostratigraphic and vitrinite reflectance data in the form of graphs, maps and correlation panels of the different stratigraphic units built for different times has proven to be a valuable tool in deciphering the tectono-thermal evolution of a basin.

In addition to the factors discussed by previous authors, the absence of economically viable hydrocarbon findings in this region might result from the hydrothermal origin of the heat that produced the organic matter maturation within the Jurassic succession. Thus, the oil and gas generation windows would have been reached in relatively small regions, close to the faults that acted as conduits for hot fluids, preventing the generation of large volumes of hydrocarbons.

The tectono-thermal evolution of the Asturian Basin proposed here challenges some aspects of previous models for the Jurassic-Cretaceous hyper-extended margin of the Bay of Biscay, regarding the structural position of the onshore portion of the Asturian Basin within the rift and the role of the Ventaniella Fault. Firstly, the small amount of extension experienced by the emerged part of the Asturian Basin suggests that it must have been situated in a proximal domain rather than in a necking domain. Secondly, the displacement along the Ventaniella Fault during the Mesozoic extensional events appears to have been small or even null, and thus, it may not have been able to behave as a major tectonic boundary during the formation of the Bay of Biscay.

CRediT authorship contribution statement

Hodei Uzkeda: Writing – review & editing, Writing – original draft, Visualization, Validation, Resources, Project administration, Methodology, Investigation, Formal analysis, Conceptualization. **Josep Poblet:** Writing – review & editing, Writing – original draft, Validation, Resources, Project administration, Methodology, Investigation, Funding acquisition, Conceptualization. **Mayte Bulnes:** Writing – review & editing, Writing – original draft, Validation, Resources, Project administration, Methodology, Investigation, Conceptualization.

Declaration of competing interest

The authors declare that they have no known competing financial

interests or personal relationships that could have appeared to influence the work reported in this paper.

Acknowledgments

We acknowledge financial support by the grant AYUD/2021/51293 funded by the Government of Asturias, and the research project PID2021-126357NB-100 funded by the Spanish Ministry of Science and Innovation. We thank J. C. García-Ramos, L. Piñuela and L. P. Fernández González for their help with stratigraphic issues. Also, we would like to thank the editor Ali Faghih and a reviewer, whose comments and suggestions have substantially improved the manuscript.

Data availability

The data used for the research are included in the article.

References

Allen, P.A., Allen, J.R., 2013. Basin analysis. Principles and Application to Petroleum Play Assessment. John Wiley & Sons, Chichester, p. 642.

Aller, J., 1986. La estructura del sector meridional de las unidades del Aramo y la Cuenca Carbonífera Central. Consejería de Industria y Comercio del Prinpicado de Asturias, p. 180. Oviedo.

Aller, J., Álvarez-Marrón, J., Bastida, F., Bulnes, M., Heredia, N., Marcos, A., Pérez-Estaún, A., Pulgar, J.A., Rodríguez-Fernández, R., 2004. Estructura, deformación y metamorfismo (Zona Cantábrica). In: Vera, J.A. (Ed.), Geología de España. Sociedad Geológica de España-Instituto Geológico y Minero de España, Madrid, pp. 42–49.

Almela, A., Rios, J.M., 1962. Investigación del hullero bajo los terrenos mesozoicos de la costa cantábrica. Empresa Nacional Adaro Investigaciones Mineras.

Alonso, J.L., Aller, J., Bastida, F., Marcos, A., Marquínez, J., Pérez-Estaún, A., Pulgar, J. A., Rodríguez Fernández, L.R., 1987–88. Mapa Geológico de España. Escala 1: 200.000. Hoja: 2 Avilés. Instituto Tecnológico Geominero de España, Madrid.

Alonso, J.L., Barrón, E., González Fernández, B., Menéndez Casares, E., García-Ramos, J. C., 2016. Extensión e inversión tectónica alpinas en el área de Sariego. Control ejercido por la estructura varisca subyacente (Asturias, norte de España). Trab. Geol. 35, 45–60.

Alonso, J.L., Gallastegui, J., García-Ramos, J.C., Poblet, J., 2009a. Estructuras mesozoicas y cenozoicas relacionadas con la apertura y cierre parcial del Golfo de Vizcaya (Zona Cantábrica–Asturias). Guía de campo, 6° Simposio sobre el margen Ibérico Atlántico (MIA09), p. 18. Oviedo.

Alonso, J.L., Marcos, A., Suárez, A., 2009b. Paleogeographic inversion resulting from large out of sequence breaching thrusts: the león fault (cantabrian zone, NW Iberia). A new picture of the external variscan thrust belt in the ibero-armorican arc. Geol. Acta 7 (4), 451–473.

Alonso, J.L., Pulgar, J.A., García-Ramos, J.C., Barba, P., 1996. Tertiary basins and alpine tectonics in the cantabrian mountains (NW Spain). In: Friend, P.F., Dabrio, C.J. (Eds.), Tertiary Basins of Spain: the Stratigraphic Record of Crustal Kinematics. Cambridge University Press, Cambridge, pp. 214–227.

Alonso López, M., 2014. Análisis estructural de los materiales jurásicos de la playa de El Rinconín, Gijón. Universidad de Oviedo, p. 47. MSc thesis.

Álvarez-Marrón, J., Hetzel, R., Niedermann, S., Menéndez, R., Marquínez, J., 2008. Origin, structure and exposure history of a wave-cut platform more than 1 Ma in age at the coast of northern Spain: a multiple cosmogenic nuclide approach. Geomorphology 93 (3–4), 316–334.

Álvarez-Marrón, J., Rubio, E., Torné, M., 1997. Subduction-related structures in the North Iberian margin. J. Geophys. Res. Solid Earth 102 (B10), 22497–22511.

Angevine, C.L., Heller, P.L., Paola, C., 1990. Quantitative sedimentary basin modeling. Continuing Education, Course Note Series # 32. American Association of Petroleum Geologists, Tulsa, p. 133.

Arbizu, M., Aller, J., Méndez-Bedia, I., 1995. Rasgos geológicos de la región de Cabo Peñas. In: Aramburu, C., Bastida, F. (Eds.), Geología de Asturias. Ediciones Trea, Gijón, pp. 231–246.

Arbizu, M., Méndez-Bedia, I., Turrero, P., 2015. CA023: Sección del Carbonífero y Cretácico en la playa de San Pedro de Antromero. Inventario Español de Lugares de Interés Geológico. Instituto Geológico y Minero de España. https://info.igme.es/ielig/LIGInfo.aspx?codigo=CA023. (Accessed 8 March 2024).

Asti, R., Saspiturry, N., Angrand, P., 2022. The Mesozoic Iberia-Eurasia diffuse plate boundary: a wide domain of distributed transtensional deformation progressively focusing along the North Pyrenean Zone. Earth Sci. Rev. 230, 104040.

Aurell, M., Meléndez, G., Olóriz, F., Bádenas, B., Caracuel, J., García-Ramos, J.C., Goy, A., Linares, A., Quesada, S., Robles, S., Rodríguez-Tovar, F.J., Rosales, I., Sandoval, J., Suárez de Centi, C., Tavera, J.M., Valenzuela, M., 2002. Jurassic. In: Gibbons, W., Moreno, T. (Eds.), The Geology of Spain. The Geological Society, London, pp. 213–253.

Bádenas, B., Armendáriz, M., Rosales, I., Aurell, M., Piñuela, L., García-Ramos, J.C., 2013. Origen de los black sales del Pliensbachiense inferior de la Cuenca Asturiana (España). Rev. Soc. Geol. Espana 26 (1), 41–54.

Barker, C.E., Pawlewicz, M.J., 1986. The correlation of vitrinite reflectance with maximum temperature in humic organic matter. Lect. Notes Earth Sci. 5, 79–93.

Barker, C.E., Pawlewicz, M.J., 1994. Calculation of vitrinite reflectance from thermal histories and peak temperatures: a comparison of methods. In: Mukhopadhyay, P., Dow, W.G. (Eds.), Vitrinite Reflectance as a Maturity Parameter, ACS Symposium Series. American Chemical Society, Washington DC, pp. 216–229.

Barrón, E., Gómez, J.J., Goy, A., 2002. Los materiales del tránsito Triásico-Jurásico en la región de Villaviciosa (Asturias, España). Caracterización palinológica. Geogaceta 31, 197–200.

Barrón, E., Gómez, J.J., Goy, A., Pieren, A.P., 2006. The Triassic-Jurassic boundary in Asturias (northern Spain): palynological characterisation and facies. Rev. Palaeobot. Palynol. 138 (3–4), 187–208.

Beroiz, C., Barón, A., Ramírez del Pozo, J., Giannini, G., Gervilla, M., 1972a. Mapa Geológico de España. Escala 1:50.000. Hoja: 30 Villaviciosa. Instituto Geológico y Minero de España, Madrid.

Beroiz, C., Pignatelli, R., Felgueroso, C., Ramírez del Pozo, J., Giannini, G., Gervilla, M., 1972b. Mapa Geológico de España. Escala 1:50.000. Hoja: 29 Oviedo. Instituto Geológico y Minero de España, Madrid.

Beroiz, C., Ramírez del Pozo, J., Giannini, G., Barón, A., Julivert, M., Truyols, J., 1972c. Mapa Geológico de España. Escala 1:50.000. Hoja: 14 Gijón. Instituto Geológico y Minero de España, Madrid.

Boillot, G., Dupeuble, P.A., Malod, J., 1979. Subduction and tectonics on the continental margin off Northern Spain. Mar. Geol. 32, 53–70.

Cadenas, P., Fernández-Viejo, G., 2017. The Asturian Basin within the North iberian margin (Bay of Biscay): seismic characterisation of its geometry and its mesozoic and cenozoic cover. Basin Res. 29, 521–541.

Cadenas, P., Fernández-Viejo, G., Pulgar, J.A., Tugend, J., Manatschal, G., Minshull, T.A., 2018. Constraints imposed by rift inheritance on the compressional reactivation of a hyperextended margin: mapping rift domains in the North Iberian Margin and in the Cantabrian Mountains. Tectonics 37, 758–785.

Cadenas, P., Manatschal, G., Fernández-Viejo, G., 2020. Unravelling the architecture and evolution of the inverted multi-stage North Iberian-Bay of Biscay rift. Gondwana Res. 88, 67–87.

Catuneanu, O., Bhattacharya, J.P., Blum, M.D., Dalrymple, R.W., Eriksson, P.G., Fielding, C.R., Fisher, W.L., Galloway, W.E., Gianolla, P., Gibling, M.R., Giles, K.A., Holbrook, J.M., Jordan, R., Kendall, C.G. St C., Macurda, B., Martinsen, O.J., Miall, A.D., Nummedal, D., Posamentier, H.W., Pratt, B.R., Shanley, K.W., Steel, R.J., Strasser, A., Tucker, M.E., 2010. Sequence stratigraphy: common ground after three decades of development. First Break 28, 21–34.

Comas-Rengifo, M.J., Goy, A., 2010. Caracterización biocronoestratigráfica del Sinemuriense Superior y el Pliensbachiense entre los afloramientos de Playa de Vega y Lastres (Asturias). Comunicaciones del V Congreso Jurásico de España, Colunga, pp. 10–18.

Comas-Rengifo, M.J., García-Martínez, J.C., Goy, A., 2010. Upper Sinemurian in Rodiles (Asturias): Biochronostratigraphy and Ammonite Biohorizons. Comunicaciones del V Congreso del Jurásico de España, Colunga, pp. 49–57.

Comas-Rengifo, M.J., García-Ramos, J.C., Piñuela, L., Gómez, J.J., Paredes, R., Suárez-Vega, L.C., 2023. El Sinemuriense superior: cronozonas Obtusum y Oxynolum en Asturias, España. Stratigraphy and Biochronostratigraphy of the Lower Pliensbachian (Jurassic) from the Asturian basin (Northern Spain). J. Iber. Geol. 49, 73–96.

Davies, R.J., O'Donnell, D., Bentham, P.N., Gibson, J.P.C., Curry, M.R., Dunay, R.E., Maynard, J.R., 1999. The origin and genesis of major Jurassic unconformities within the triple junction area of the North Sea, UK. In: Fleet, A.J., Boldy, S.A.R. (Eds.), Petroleum Geology of Northwest Europe: Proceedings of the 5th Conference. The Geological Society, London, pp. 117–131.

De Vicente, G., Cloetingh, S., Van Wees, J.D., Cunha, P.P., 2011. Tectonic classification of Cenozoic Iberian foreland basins. Tectonophysics 502, 38–61.

Dembicki Jr., H., 2009. Three common source rock evaluation errors made by geologists during prospect or play appraisals. AAPG (Am. Assoc. Pet. Geol.) Bull. 93 (3), 341–356.

Dembicki, H. Jr, 2022. Practical Petroleum Geochemistry for Exploration and Production, second ed. Elsevier, p. 415.

Dow, W., 1977. Kerogen studies and geological interpretations. J. Geochem. Explor. 7, 79–99.

Dubar, G., Mouterde, R., 1957. Extension du Kimméridgien marin dans les Asturies depuis Ribadesella jusqu'a Gijón. Comptes Rendus Hebdomadaires des Séances de l'Académie des Sciences 244 (1), 99–101.

Ernst, W.G., Ferreiro Mählman, R., 2004. Vitrinite Alteration Rate as a Function of Temperature, Time, Starting Material, Aqueous Fluid Pressure and Oxygen Fugacity – Laboratory Corroboration of Previous Work, vol. 9. The Geochemical Society Special Publications, pp. 341–357.

Fernández-López, S., Suárez-Vega, L.C., 1981. Estudio bioestratigráfico (Ammonoidea) del Aaleniense y Bajociense en Asturias. Estud. Geol. 35 (1–6), 231–239.

Fernández-Viejo, G., Llana-Fúnez, S., Acevedo, J., López-Fernández, C., 2021. The Cantabrian Fault at sea. Low magnitude seismicity and its significance within a stable setting. Front. Earth Sci. 9, 645061.

Fernández-Viejo, G., López Fernández, C., Domínguez-Cuesta, M.J., Cadenas, P., 2014. How much confidence can be conferred on tectonic maps of continental shelves? The Cantabrian-Fault case. Sci. Rep. 4, 3661.

Fillon, C., Pedreira, D., Van Der Beek, P.A., Huismans, R.S., Barbero, L., Pulgar, J.A., 2016. Alpine exhumation of the central Cantabrian mountains, northwest Spain. Tectonics 35 (2), 339–356.

Flor, G., 1983. Las rasas asturianas: ensayos de correlación y emplazamiento. Trab. Geol. 13, 65–83.

Flórez Rodríguez, A.G., 2024. Reactivación de fallas en Picos de Europa (Zona Cantábrica) deducida a partir del análisis estructural y la caracterización de

paleofluidos y mineralizaciones asociadas. Universidad de Oviedo, p. 229. PhD Thesis.
Fürsich, F.T., Werner, W., Delvene, G., García-Ramos, J.C., Bermúdez-Rochas, D.D., Piñuela, L., 2012. Taphonomy and palaeoecology of high-stress benthic associations from the Upper Jurassic of Asturias, northern Spain. Palaeogeogr. Palaeoclimatol. Palaeoecol. 358–360, 1–18.
Gallastegui, J., 2000. Estructura cortical de la cordillera y margen continental cantábricos: perfiles ESCI-N. Trab. Geol. 22, 3–234.
García-Ramos, J.C., Gutiérrez Claverol, M., 1995. La cobertera mesozoico-terciaria. In: Aramburu, C., Bastida, F. (Eds.), Geología de Asturias. Ediciones Trea, Gijón, pp. 81–94.
García-Ramos, J.C., Piñuela, L., Bádenas, B., Aurell, M., 2010a. Ciclos elementales de escala milenaria en una ritmita de margacaliza del Pliensbachiense de Asturias (Formación Rodiles). Comunicaciones del V Congreso del Jurásico de España, Colunga, pp. 73–82.
García-Ramos, J.C., Piñuela, L., Aramburu, C., 2010b. La Formación Tereñes en su localidad tipo. In: García-Ramos, J.C., Aramburu, C. (Eds.), Las sucesiones litorales y marinas restringidas del Jurásico Superior. Acantilados de Tereñes (Ribadesella) y de la playa de La Griega (Colunga): Guía de la excursión B del V Congreso del Jurásico de España, Colunga, pp. 15–40.
García-Ramos, J.C., Piñuela, L., Lires, J.F., 2006. Atlas del Jurásico de Asturias. Ediciones Nobel, Oviedo, p. 225.
García-Ramos, J.C., Piñuela, L., Rodríguez-Tovar, F.J., 2011. Field Trip Guide. XI International Ichnofabric Workshop, Colunga, p. 89.
García-Ramos, J.C., Piñuela, L., Uzkeda, H., Poblet, J., Bulnes, M., Alonso, J.L., Suárez-Vega, L.C., 2010c. Travertinos ricos en oncoides asociados a paleomanantiales y lagos efímeros próximos a fallas sinsedimentarias en el Jurásico Superior de Asturias. Comunicaciones del V Congreso del Jurásico de España, Colunga 83–91.
García-Ramos, J.C., Suárez de Centi, C., Valenzuela, M., 1992. Icnofósiles, sedimentación episódica, tempestitas fangosas y "black sales" de ambientes seudoanóxicos, en sucesiones marinas de plataforma y rampa. Geogaceta 12, 99–100.
García-Ramos, J.C., Valenzuela, M., Aramburu, C., 1979. Descripción e interpretación de ciclos fluviales en el Jurásico de Asturias. Cuadernos de Geología 10, 23–33.
Gómez, J.J., Comas-Rengifo, M.J., Goy, A., 2016a. Palaeoclimatic oscillations in the pliensbachian (early jurassic) of the Asturian basin. Climate in the Past 12, 1199–1214.
Gómez, J.J., Comas-Rengifo, M.J., Goy, A., 2016b. The hydrocarbon source rocks of the Pliensbachian (early Jurassic) in the Asturian Basin (northern Spain): their relationship with the palaeoclimatic oscillations and gamma-ray response. J. Iber. Geol. 42, 259–273.
González-Fernández, B., Menéndez Casares, E., García-Ramos, J.C., 2004a. Subunidades litoestratigráficas de la Formación Gijón (Triásico Superior-Jurásico Inferior) en Asturias. Geotemas 6, 71–74.
González-Fernández, B., Menéndez Casares, E., Gutiérrez Claverol, M., García-Ramos, J. C., 2004b. Litoestratigrafía del sector occidental de la cuenca cretácica de Asturias. Trab. Geol. 24, 43–80.
González-Fernández, B., Menéndez-Casares, E., Vicedo, V., Aramburu, C., Caus, E., 2014. New insights about the upper jurassic – lower cretaceous sedimentary successions from Asturias (NW iberian Peninsula). J. Iber. Geol. 40 (3), 409–430.
Goy, A., Comas-Rengifo, M.J., Gómez, J.J., Herrero, C., Suárez-Vega, L.C., Ureta, S., 2010. Toarcian Ammonite Biohorizons in Asturias. Comunicaciones del V Congreso del Jurásico de España, Colunga, pp. 94–102.
Grobe, R.W., Alvarez-Marrón, J., Glasmacher, U.A., Menéndez-Duarte, R., 2010. Low-temperature exhumation history of Variscan-age rocks in the western Cantabrian Mountains (NW Spain) recorded by apatite fission-track data. Tectonophysics 489 (1–4), 76–90.
Gutiérrez Claverol, M.A., Gallastegui, J., 2002. Prospección de hidrocarburos en la plataforma continental de Asturias. Trab. Geol. 23, 21–34.
Gutiérrez Claverol, M., Fernández, C.L., Alonso, J.L., 2006. Procesos neotectónicos en los depósitos de rasa de la zona de Canero (Occidente de Asturias). Geogaceta 40, 75–78.
Gutiérrez Claverol, M.A., Luque Cabal, C., Sáenz de Santa María, J.A., 2005. Manifestaciones de hidrocarburos gaseosos en Asturias. Trab. Geol. 25, 51–67.
Gutiérrez Claverol, M., Torres-Alonso, M., Luque-Cabal, C., 2002. El subsuelo de Gijón. *Aspectos Geológicos*. CQ Licer. S.L., Oviedo, p. 462.
Hallam, A., 2001. A review of the broad pattern of Jurassic sea-level changes and their possible causes in the light of current knowledge. Palaeogeogr. Palaeoclimatol. Palaeoecol. 167 (1–2), 23–37.
Handy, R.M., Schmid, S.M., Bousquet, R., Kissling, E., Bernoulli, D., 2010. Reconciling plate-tectonic reconstructions of Alpine Tethys with the geological-geophysical record of spreading and subduction in the Alps. Earth Sci. Rev. 102 (3–4), 121–156.
Hardenbol, J., Thierry, J., Farley, M.B., Jacquin, T., De Graciansky, P.C., Vail, P.R., 1998. Mesozoic and Cenozoic sequence chronostratigraphic framework of European basins. Society of Economic Paleontologists and Mineralogist Special Publication 60, 3–13.
Haq, B.U., 2018. Jurassic sea-level variations: a reappraisal. GSA Today (Geol. Soc. Am.) 28 (1), 4–10.
Haq, B.U., Hardenbol, J., Vail, P.R., 1987. Chronology of fluctuating sea levels since the Triassic. Science 235, 1156–1167.
International Commission on Stratigraphy, 2023. International chronostratigraphic Chart. https://stratigraphy.org/chart. (Accessed 21 November 2023).
Jammes, S., Manatschal, G., Lavier, L., Masini, E., 2009. Tectonosedimentary evolution related to extreme crustal thinning ahead of a propagating ocean: example of the western Pyrenees. Tectonics 28, TC4012.
Jiménez, A., Iglesias, M.J., Laggoun-Défarge, F., Suárez-Ruiz, I., 1998. Study of physical and chemical properties of vitrinites. Inferences on depositional and coalification controls. Chem. Geol. 150, 197–221.
Julivert, M., 1971. Décollement tectonics in the hercynian cordillera of NW Spain. Am. J. Sci. 270, 1–29.
Julivert, M., 1983. La estructura de la Zona Cantábrica. In: Comba, J.A. (Ed.), Geología de España. Libro Jubilar J. M. Ríos, Tomo I. Instituto Geológico y Minero de España, Madrid, pp. 339–381.
Julivert, M., Pello, J., 1970. Mapa Geológico de España. Escala 1:200.000. Síntesis de la cartografía existente. Hoja: 3 Oviedo. Instituto Geológico y Minero de España, Madrid.
Julivert, M., del Pozo, J.R., Truyols, J., 1971. Le réseau de failles et la couverture post-hercynienne dans les Asturies. Editions Technip, Paris.
Julivert, M., Fontboté, J.M., Ribeiro, A., Conde, L.E., 1972a. Mapa Tectónico de la Península Ibérica y Baleares, Escala 1:1.000.000. Instituto Geológico y Minero de España, Madrid.
Julivert, M., Truyols, M., Marcos, A., Arboleya, M.A., 1972b. Mapa Geológico de España. Escala 1:50.000. Hoja: 13 Avilés. Instituto Geológico y Minero de España, Madrid.
King, M.T., Welford, J.K., Cadenas, P., Tugend, J., 2021. Investigating the plate kinematics of the Bay of Biscay using deformable plate tectonics models. Tectonics 40, e2020TC006467.
King, M.T., Welford, J.K., Tugend, J., 2023. The role of the Ebro Block on the deformation experienced within the Pyrenean realm: insights from deformable plate tectonics model. J. Geodyn. 155, 101962.
Le Pichon, X., Sibuet, J.C., 1971. Western extension of boundary between European and Iberian plates during the Pyrenean orogeny. Earth Planet Sci. Lett. 12 (1), 83–88.
Lepvrier, C., Martínez-García, E., 1990. Fault development and stress evolution of the post-Hercynian Asturian Basin (Asturias and Cantabria, northwestern Spain). Tectonophysics 184 (3–4), 345–356.
López-Fernández, C., Fernández-Viejo, G., Olona, J., Llana-Fúnez, S., 2018. Intraplate seismicity in northwest Iberia along the trace of the Ventaniella fault: a case for fault intersection at depth. Bull. Seismol. Soc. Am. 108, 604–618.
López-Fernández, C., Llana-Fúnez, S., Fernández-Viejo, G., Domínguez-Cuesta, M.J., Díaz-Díaz, L.M., 2020. Comprehensive characterization of elevated coastal platforms in the north Iberian margin: a new template to quantify uplift rates and tectonic patterns. Geomorphology 364, 1072742.
López-Fernández, C., Pulgar, J.A., Gallart, J., González-Cortina, J.M., Díaz, J., Ruiz, M., 2004. Actividad sísmica en el noroeste de la Península Ibérica observada por la red sísmica local del Proyecto GASPI (1999-2002). Trab. Geol. 24, 91–107.
López-Gómez, J., Martín-González, F., Heredia, N., de la Horra, R., Barrenechea, J.F., Cadenas, P., Juncal, M., Diez, J.B., Borruel-Abadía, V., Pedreira, D., García-Sansegundo, J., Farias, P., Galé, C., Lago, M., Ubide, T., Fernández-Viejo, G., Gand, G., 2019. New lithostratigraphy for the Cantabrian Mountains: a common tectono-stratigraphic evolution for the onset of the Alpine cycle in the W Pyrenean realm, N Spain. Earth-Sciences Reviews 188, 249–271.
Lotze, F., 1945. Zur gliederung der variszíden der Iberischen Meseta. Geotekt. Forsch. 6, 78–92.
Magán, M., 2017. Análisis de la fracturación en un anticlinal desarrollado en rocas jurásicas en la playa Peñarrubia, Gijón (Cuenca Asturiana, NO de la Península Ibérica). Universidad de Oviedo, p. 53. MSc thesis.
Magán, M., 2024. Desarrollo de una base de datos y herramientas para el análisis estructural de datos de campo y de modelos de afloramientos virtuales: aplicación a rocas jurásicas deformadas de la costa de Gijón (Cuenca Asturiana, N de la Península Ibérica). Universidad de Oviedo, p. 267. PhD thesis.
Magán, M., Bulnes, M., Poblet, J., 2022a. A tool to explore slip/separation relationships in faults that offset inclined or folded surfaces. Examples from the Asturian Basin (NW Iberian Peninsula). Bull. Geol. Soc. Greece. *Special Publication*, 10: Ext. Abs. GSG2022-028.
Magán, M., Poblet, J., Bulnes, M., 2022b. Tools to analyse misleading kinematic interpretations of faults offsetting inclined or folded surfaces: applications to Asturian Basin (NW Iberian Peninsula) examples. J. Struct. Geol. 162, 104687.
Martín, S., Uzkeda, H., Poblet, J., Bulnes, M., Rubio, R., 2013. Construction of accurate geological cross-sections along trenches, cliffs and mountain slopes using photogrammetry. Comput. Geosci. 51, 90–100.
Martínez-Álvarez, J.A., Gutiérrez Claverol, M., Torres-Alonso, M., 1972. Mapa Geológico de España. Escala 1:50.000. Hoja: 28 Grado. Instituto Geológico y Minero de España, Madrid.
Mary, G., 1983. Evolución del margen costero de la Cordillera Cantábrica en Asturias desde el Mioceno. Trab. Geol. 13, 3–37.
Merino-Tomé, O., Suárez-Rodríguez, A., Alonso, J.L., 2023. Mapa geológico digital continuo E. 1:50.000, zona cantábrica (Zona-1000). In: GEODE. Mapa Geológico Digital conitnuo de España. http://info.igme.es/cartografiadigital/geologica/geodezona.aspx?Id=Z1000. (Accessed 21 November 2023).
Miller, K.G., Browning, J.V., Schmelz, W.J., Kopp, R.E., Mountain, G.S., &Wright, J.D., 2020. Cenozoic sea-level and cryospheric evolution from deep-sea geochemical and continental margin records. Sci. Adv. 6 (20), eaaz1346.
Navarro, D., Rodríguez Fernández, L.R., 1984. Mapa Geológico de España. Escala 1: 50.000. Hoja: 31 Ribadesella. Instituto Tecnológico Geominero de España, Madrid.
Odriozola Zubillaga, M.J., 2016. Extensión y compresión en los materiales jurásicos de la playa de Peñarrubia, Gijón. Universidad de Oviedo, p. 31. MSc thesis.
Olivet, J.L., 1996. Kinematics of the Iberian Plate. Bull. Cent. Rech. Explor.-Prod. Elf-Aquitaine 20 (1), 131–195.
Olóriz, F., Valenzuela, M., García-Ramos, J.C., Suárez de Centi, C., 1988. The first record of the genus Eurasenia (ammonitina) from the upper Jurassic of Asturias (northern Spain). Geobios 21 (6), 741–748.

Pérez-Estaún, A., Bastida, F., 1990. Cantabrian zone: structure. In: Dallmeyer, R.D., Martínez-García, E. (Eds.), Pre-Mesozoic Geology of Iberia. Springer-Verlag, Berlin, pp. 55–69.
Pérez-Estaún, A., Bastida, F., Alonso, J.L., Marquínez, J., Álvarez-Marrón, J., Marcos, A., Pulgar, J.A., 1988. A thin-skinned tectonics model for an arcuate fold and thrust belt: the Cantabrian Zone (Variscan Ibero-Armorican Arc). Tectonics 7, 517–537.
Pieren, A.P., Areces, J.L., Toraño, J., Martínez-García, E., 1995. Estratigrafía y estructura de los materiales permotriásicos del sector Gijón-La Collada (Asturias). Cuad. Geol. Iber. 19, 309–335.
Pignatelli, R., Giannini, G., Ramírez del Pozo, J., Beroiz, C., Barón, A., 1972. Mapa Geológico de España. Escala 1:50 000, Hoja: 15 Lastres. Instituto Geológico y Minero de España, Madrid.
Pulgar, J.A., Alonso, J.L., Espina, R.G., Marín, J.A., 1999. La deformación alpina en el basamento varisco de la Zona Cantábrica. Trab. Geol. 21, 283–294.
Riaza Molina, C., 1996. Inversión estructural en la cuenca mesozoica del off-shore asturiano. Revisión de un modelo exploratorio. Geogaceta 20 (1), 169–171.
Roca, E., Muñoz, J.A., Ferrer, O., Ellouz, N., 2011. The role of the Bay of Biscay Mesozoic extensional structure in the configuration of the Pyrenean orogen: constraints from the MARCONI deep seismic reflection survey. Tectonics 30 (2), TC2001.
Saénz de Santamaría, J., Gutiérrez Claverol, M.G., 2013. Valoración de la técnica de fracturación hidráulica y su aplicación a la extracción de gas no convencional en las cuencas carbonífera y jurásica de Asturias. Trab. Geol. 33, 51–67.
Sánchez de la Torre, L., Águeda Villa, J.A., Colmenero, J.R., Manjón, M., 1977. La serie permotriásica en la región de Villaviciosa (Asturias). Cuad. Geol. Iber. 4, 329–338.
Sánchez de la Torre, L., Barba Regidor, F.J., 1981. Estudio sedimentológico de los conglomerados del Jurásico de Asturias (borde occidental). Trab. Geol. 11, 203–212.
Sánchez, V., Cardellach, E., Corbella, M., Vindel, E., Martín-Crespo, T., Boyce, A.J., 2010. Variability in fluid sources in the fluorite deposits from Asturias (N Spain): further evidences from REE, radiogenic (Sr, Sm, Nd) and stable (S, C, O) isotope data. Ore Geol. Rev. 37 (2), 87–100.
Sánchez, V., Corbella, M., Fuenlabrada, J.M., Vindel, E., Martín-Crespo, T., 2006. Sr and Nd isotope data from the fluorspar district of Asturias, northern Spain. J. Geochem. Explor. 89 (1–3), 348–350.
Sánchez, V., Vindel, E., Martín-Crespo, T., Corbella, M., Cardellach, E., Banks, D., 2009. Sources and composition of fluids associated with fluorite deposits of Asturias (N Spain). Geofluids 9, 338–355.
Savage, J.F., 1979. The hercynian orogeny in the cantabrian mountains, northern Spain. Krystalinikum 14, 91–108.
Savage, J.F., 1981. Geotectonic cross-section through the Cantabrian mountains, northern Spain. Geol. Mijnbouw 81, 3–5.
Schmoker, J.W., Halley, R.B., 1982. Carbonate porosity versus depth: a predictable relation for south Florida. AAPG (Am. Assoc. Pet. Geol.) Bull. 66 (12), 2561–2570.
Schudack, M., Schudack, U., 2002. New biostratigraphical data for the upper jurassic of Asturias (northern Spain) based on ostracoda. Rev. Espanola Micropaleontol. 34 (1), 1–18.
Sclater, J.G., Christie, P., 1980. Continental stretching: an explanation of the post-mid-Cretaceous subsidence of the central North Sea basin. J. Geophys. Res. Solid Earth 85 (B7), 3711–3739, 1978, 2012.
Senftle, J.T., Landis, C.R., 1991. Vitrinite reflectance as a tool to assess thermal maturity. In: Merrill, R.K. (Ed.), Source and Migration Processes and Evaluation Techniques. AAPG Treatise of Petroleum Geology, Handbook of Petroleum Geology, pp. 119–125.
Sibuet, J.-C., Srivastava, S.P., Spakman, W., 2004. Pyrenean orogeny and plate kinematics. J. Geophys. Res. 109 (B8), B08104.
Srivastava, S.P., Sibuet, J.C., Cande, S., Roest, W.R., Reid, I.D., 2000. Magnetic evidence for slow seafloor spreading during the formation of the Newfoundland and Iberian margins. Earth Planet Sci. Lett. 182 (1), 61–76.
Stampfli, G.M., Borel, G.D., Marchant, R., Mosar, J., 2002. Western Alps geological constraints on western Tethyan reconstructions. J. Virtual Explor. 8, 77–106.
Suárez-Rodríguez, Á., 1988. Estructura del área de Villaviciosa-Libardón (Asturias, Cordillera Cantábrica). Trab. Geol. 17, 87–98.
Suárez-Ruiz, I., 1988. Caracterización, clasificación y studio de la evolución de la materia orgánica dispersa (MOD) en el Jurásico de Asturias y Cantabria. PhD thesis. Universidad de Oviedo, p. 372.
Suárez-Ruiz, I., González Prado, J., 1995. Characterization of Jurassic black shales from Asturias (northern Spain): evolution and petroleum potential. In: Snape, C. (Ed.), Composition, Geochemistry and Conversion of Oil Shales. Kluwer Academic Publishers, Dordrecht, pp. 387–393.
Suárez-Ruiz, I., Iglesias, M.J., Jiménez, A., Cuesta, M.J., Laggoun-Défarge, F., 2006. El azabache de Asturias: características físico-químicas, propiedades y génesis. Trab. Geol. 26, 9–18.
Suárez-Ruiz, I., Iglesias, M.J., Jiménez Bautista, A., Laggoun-Défarge, F., Prado, J.G., 1994. Petrographic and geochemical anomalies detected in the Spanish Jurassic jet. In: Mukhopadhyay, P.K., Dow, W.G. (Eds.), Vitrinite Reflectance as a Maturity Parameter. Applications and Limitations, vol. 6. American Chemical Society Symposium Series. ACS Books, pp. 76–92, 570.
Suárez-Vega, L.C., 1974. Estratigrafía del Jurásico de Asturias. Cuad. Geol. Iber. 74 (3), 1–369.
Suess, E., 1892. Das Antlitz der Erde. F. Tempsky, Wien.
Tugend, J., Manatschal, G., Kusznir, N., 2015a. Spatial and temporal evolution of hyperextended rift systems: implication for the nature, kinematics, and timing of the Iberian-European plate boundary. Geology 43 (1), 15–18.
Tugend, J., Manatschal, G., Kusznir, N.J., Masini, E., 2015b. Characterizing and identifying structural domains at rifted continental margins: application to the Bay of Biscay margins and its Wester Pyrenean forssil remnants. In: Gibson, G.M., Roure, F., Manatschal, G. (Eds.), Sedimentary Basins and Crustal Processes at Continental Margins: from Modern Hyper-Extended Margins to Deformed Ancient Analogues, vol. 413. Geological Society, London, Special Publications, pp. 171–203.
Underhill, J.R., Partington, M.A., 1993. Jurassic thermal doming and deflation in the North Sea: implications of the sequence stratigraphic evidence. In: Parker, J.R. (Ed.), Petroleum Geology of Northwest Europe: Proceedings of the 4th Conference. The Geological Society, London, pp. 337–345.
Uzkeda, H., 2013. Reconstrucción 3D y análisis estructural de las rocas jurásicas de Colunga-Tazones (Cuenca Asturiana, NO de la Península Ibérica). Universidad de Oviedo, p. 259. PhD thesis.
Uzkeda, H., Bulnes, M., Poblet, J., García-Ramos, J.C., Piñuela, L., 2013. Buttressing and reverse reactivation of a normal fault in the Jurassic rocks of the Asturian Basin, NW Iberian Peninsula. Tectonophysics 599, 117–134.
Uzkeda, H., Bulnes, M., Poblet, J., García-Ramos, J.C., Piñuela, L., 2016. Jurassic extension and Cenozoic inversion tectonics in the Asturian Basin, NW Iberian Peninsula: 3D structural model and kinematic evolution. J. Struct. Geol. 90, 157–176.
Uzkeda, H., Bulnes, M., Poblet, J., García-Ramos, J.C., Piñuela, L., Martín, S., 2012. Un ejemplo de inversión tectónica (tipo contrafuerte) en las rocas jurásicas de la Cuenca Asturiana: Ensenada de la Conejera (Villaviciosa). Resúmenes extendidos del VIII Congreso Geológico de España, CD anexo a Geo-Temas 13, 457–460.
Uzkeda, H., Poblet, J., Bulnes, M., García-Ramos, J.C., Piñuela, L., 2015. Extension and inversion of jurassic hydrocarbon source rocks in the NE part of the Asturian basin, NW iberian Peninsula. 77th EAGE Conference and Exhibition: Earth Science for Energy and Environment, pp. 4307–4311. Madrid.
Uzkeda, H., Poblet, J., Bulnes, M., Martín, S., 2018. Effects of inherited structures on inversion tectonics: examples from the Asturian basin (NW iberian Peninsula) interpreted in a computer assisted virtual environment (CAVE). Geosphere 14 (4), 1635–1656.
Uzkeda, H., Poblet, J., Magán, M., Bulnes, M., Martín, S., Fernández-Martínez, D., 2022. Virtual outcrop models: digital techniques and an inventory of structural models from north-northwest Iberia (cantabrian zone and Asturian basin). J. Struct. Geol. 157, 104568.
Valenzuela, M., 1989. Estratigrafía, sedimentología y paleogeografía del Jurásico de Asturias. Universidad de Oviedo, p. 748. PhD thesis.
Valenzuela, M., García-Ramos, J.C., Suárez de Centi, C., 1986. The jurassic sedimentation in Asturias (N Spain). Trab. Geol. 16, 121–132.
Valenzuela, M., García-Ramos, J.C., Suárez de Centi, C., 1989. La sedimentación en una rampa carbonatada dominada por tempestades, ensayos de correlación de ciclos y eventos en la ritmita margo-calcárea del Jurásico de Asturias. Cuad. Geol. Iber. 13, 217–235.
Vissers, R.L.M., Meijer, P. Th, 2012. Mesozoic rotation of Iberia: subduction in the Pyrenees? Earth Sci. Rev. 110 (1–4), 93–110.
Zamora, G., Fleming, M., Gallastegui, J., 2017. Salt tectonics within the offshore Asturian basin: north Iberian margin. In: Soto, J.I., Flinch, J.F., Tari, G. (Eds.), Permo-Triassic Salt Provinces of Europe, North Africa and the Atlantic Margins – Tectonics and Hydrocarbon Potential. Elsevier, pp. 358–368.